ChemPubSoc Europe

DOI: 10.1002/cmdc.201500284

CHEMMEDCHEM Full Papers

VIP *Very Important Paper*

Discovery, Synthesis, and Optimization of Diarylisoxazole-3-carboxamides as Potent Inhibitors of the Mitochondrial Permeability Transition Pore

Sudeshna Roy,[a] Justina Šileikytė,[b] Marco Schiavone,[b] Benjamin Neuenswander,[a] Francesco Argenton,[c] Jeffrey Aubé,[a] Michael P. Hedrick,[d] Thomas D. Y. Chung,[d] Michael A. Forte,*[e] Paolo Bernardi,*[b] and Frank J. Schoenen*[a]

The mitochondrial permeability transition pore (mtPTP) is a Ca^{2+}-requiring mega-channel which, under pathological conditions, leads to the deregulated release of Ca^{2+} and mitochondrial dysfunction, ultimately resulting in cell death. Although the mtPTP is a potential therapeutic target for many human pathologies, its potential as a drug target is currently unrealized. Herein we describe an optimization effort initiated around hit **1**, 5-(3-hydroxyphenyl)-*N*-(3,4,5-trimethoxyphenyl)isoxazole-3-carboxamide, which was found to possess promising inhibitory activity against mitochondrial swelling (EC_{50} < 0.39 μM) and showed no interference on the inner mitochondrial membrane potential (rhodamine 123 uptake EC_{50} > 100 μM). This enabled the construction of a series of picomolar mtPTP inhibitors that also potently increase the calcium retention capacity of the mitochondria. Finally, the therapeutic potential and in vivo efficacy of one of the most potent analogues, *N*-(3-chloro-2-methylphenyl)-5-(4-fluoro-3-hydroxyphenyl)isoxazole-3-carboxamide (**60**), was validated in a biologically relevant zebrafish model of collagen VI congenital muscular dystrophies.

Introduction

The vital roles of mitochondria involve ATP synthesis, redox signaling, and regulation of cytoplasmic and mitochondrial matrix calcium (Ca^{2+}) levels.[1] The latter function is reflected by the mitochondrion's high capacity to store Ca^{2+} in response to signals arising from elevated cytoplasmic Ca^{2+} concentrations.[2] The mitochondrial permeability transition pore (mtPTP) is a high-conductance channel of the inner mitochondrial membrane (IMM) sensitive to cyclosporin (Cs) A that opens transiently under normal physiological conditions, possibly acting as a mitochondrial Ca^{2+}-release channel to help maintain cellular Ca^{2+} homeostasis.[3] However, under pathological conditions, the mtPTP opens persistently and results in fatal consequences such as IMM depolarization, deregulated release of matrix Ca^{2+}, termination of oxidative phosphorylation, swelling, and eventually rupture of the outer mitochondrial membrane (OMM) with the release of apoptotic proteins, resulting in cell death.[3c,4] Persistent opening of the mtPTP may contribute to a host of chronic and therapeutically challenging diseases, such as multiple sclerosis,[5] amyotrophic lateral sclerosis,[6] Alzheimer's disease,[7] muscular dystrophies,[8] myocardial infarction,[9] stroke,[10] and diabetes.[11] A key pathophysiological hallmark in these diseases is likely based in mitochondrial dysfunction triggered by Ca^{2+} and potentiated by oxidative stress.[12]

The molecular composition of the mtPTP is still incompletely understood.[13] The previous long-standing belief that the mtPTP forms at the adjoining sites of the inner and outer membranes through association of the voltage-dependent anion channel (VDAC)[14] of the OMM and the adenine nucleotide translocator (ANT)[15] of the IMM has not been supported by rigorous genetic tests, as VDAC- and ANT-null mitochondria still display a CsA-sensitive mtPTP.[16] Over the past decade, similar genetic analyses have discounted the participation of many other components of the earlier models of the mtPTP.[17] Other studies suggest that the mtPTP forms from dimers of the F_OF_1 ATP synthase (F-ATP synthase), the IMM nanomachine responsible for the synthesis of ATP.[18] In this context, the mtPTP represents a unique, Ca^{2+}-dependent channel originating from F-ATP synthase that is highly favored by formation of disulfide bonds during oxidative stress.[19] How dimers of F-ATP

[a] *Dr. S. Roy,[+] B. Neuenswander, Prof. Dr. J. Aubé, Dr. F. J. Schoenen*
University of Kansas Specialized Chemistry Center
2304 Becker Drive, Lawrence, KS 66049 (USA)
E-mail: schoenen@ku.edu

[b] *Dr. J. Šileikytė,[+] Dr. M. Schiavone, Prof. Dr. P. Bernardi*
CNR Neuroscience Institute and Department of Biomedical Sciences
University of Padova, Padova, 35131 (Italy)
E-mail: bernardi@bio.unipd.it

[c] *Prof. Dr. F. Argenton*
Department of Biology, University of Padova, Padova, 35131 (Italy)

[d] *Dr. M. P. Hedrick, Dr. T. D. Y. Chung*
Conrad Prebys Center for Chemical Genomics
Sanford–Burnham Medical Research Institute, La Jolla, CA 92037 (USA)

[e] *Prof. Dr. M. A. Forte*
Vollum Institute
Oregon Health & Science University, Portland, OR 97239 (USA)
E-mail: forte@ohsu.edu

[+] *These authors contributed equally to this work.*

Supporting information for this article is available on the WWW under http://dx.doi.org/10.1002/cmdc.201500284.

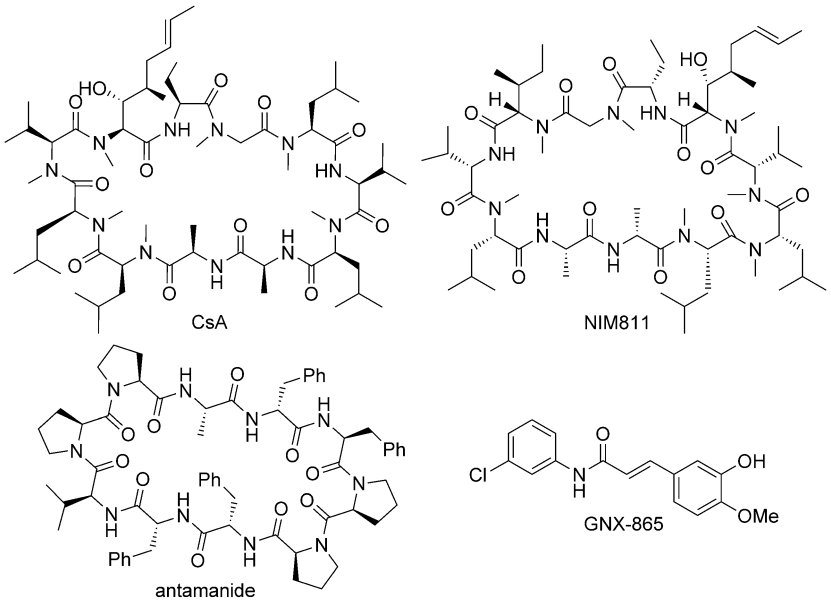

Figure 1. Structures of prominent mtPTP inhibitors.

synthase switch from a Mg^{2+}-dependent catalytic system that makes or hydrolyses ATP into a Ca^{2+}-dependent pore that eliminates the IMM transmembrane potential, which is required for ATP synthesis, remains to be established. While many mtPTP inhibitors have been reported (a few are shown in Figure 1), most of them are not selective and likely inhibit the mtPTP through indirect effects.[20] The most studied inhibitor of the mtPTP is CsA. CsA binds to cyclophilin (CyP) D, a matrix peptidylprolyl *cis–trans* isomerase (PPIase) and inhibits its activity. However, CyPD inhibitors only desensitize the mtPTP without blocking its activity, as demonstrated by the fact that the mtPTP can still open after elimination of the nuclear gene encoding CyPD.[21] CsA binds to and inhibits the action of all members of the CyP family (16 different CyP proteins are encoded by mammalian genomes).[22] As a result, through interaction with another member of this family, CyPA, CsA also mediates inhibition of calcineurin, resulting in immunosuppression, which is a major side effect of therapy for mtPTP-dependent diseases.[23] Consequently, non-immunosuppressive CyPD inhibitors (e.g., NIM811, Debio025, and antamanide)[24] derived from CsA have been used as therapeutic agents in mtPTP-dependent disease models.[25] However, all CsA derivatives inhibit all CyPs to some extent—not just the mitochondrial isoform—and, like CsA, desensitize, but do not block, the mtPTP. Furthermore, CsA and its derivatives cannot be used to treat mtPTP-based neurological diseases because they do not cross the blood–brain barrier.[23,26]

Despite the above advances, more potent and selective mtPTP inhibitors are needed for use as tool compounds and for possible drug discovery activities. Herein we report the results of a screening/chemical optimization approach that has yielded small-molecule inhibitors of the mtPTP that are ~1000-fold more potent than GNX-865 (which is one of the most relevant prior-art compounds, as reported by Fancelli et al.[27]) in the mitochondrial swelling assay and also exhibit high in vivo efficacy in a zebrafish model of collagen VI (ColVI) congenital muscular dystrophies, a biologically accurate model of a mtPTP-based disease.[28]

Results and Discussion

Identification of small-molecule mtPTP inhibitors

As a part of the Molecular Libraries Program of the US National Institutes of Health (NIH), a high-throughput screen was performed within the Molecular Libraries Probe Production Centers Network (MLPCN) to seek new structural hits for the development of potent, small-molecule inhibitors of mtPTP (PubChem Summary AID: 602491).[29] The NIH Molecular Libraries Small Molecule Repository (MLSMR) collection of 363827 compounds was screened at a concentration of 10 μM in isolated mouse liver mitochondria using the mtPTP swelling assay. Compounds were selected as hits if they were found to inhibit mitochondrial swelling by at least 50% relative to controls. Using this selection criterion, 5040 compounds were identified, corresponding to a hit rate of 1.4% (PubChem AID: 602449). These compounds were subsequently tested in the mitochondrial rhodamine (Rh) 123 uptake assay to identify and exclude probes that interfered with maintenance of the IMM potential (thus preventing Ca^{2+} uptake) rather than inhibiting the mtPTP. Compounds exhibiting >20% inhibition at 10 μM in this counter-screen assay were excluded from further consideration, which resulted in 1097 compounds of interest. This list was condensed further to 819 compounds based on cheminformatic identification of biologically promiscuous compounds (PubChem Promiscuity) and PAINS (*P*an *A*ssay *I*nterference Compounds).[30] The concentration–response effect of these compounds was measured in the mitochondrial swelling (PubChem AID: 651561) and Rh123 uptake assays (PubChem AID: 651564) and yielded 248 compounds with $EC_{50}<20$ μM in the swelling assay, and a Rh123-uptake-to-swelling EC_{50} ratio of >5-fold, benchmark criteria that were established at the outset of the project. A final prioritization of compounds was based on lack of reactive functionalities and synthetic tractability, followed by validation of activity on high-quality compound samples from the solid physical state. A total of 27 hits, along with CsA as a positive control, were assayed by the calcium retention capacity (CRC) test, a good alternative to the mitochondrial swelling assay used as the primary screen. Amongst all of the validated hits, compounds from the isoxazole chemotype exhibited activity similar to that of CsA in isolated mouse liver mitochondria and also increased the CRC of permeabilized mouse

(murine embryonic fibroblasts) and human (HeLa) cells, thereby demonstrating that their effects were not mouse-specific. Based on biological activity and physicochemical properties, the isoxazole scaffold, represented by hit compound **1** (Figure 2), was selected as a starting point for further structure–activity relationship (SAR) studies.

Isoxazole compounds are novel structural entities that target the mtPTP

Isoxazole compounds are known for their potential use in a broad array of diseases across the infectious and parasitic diseases and oncology therapeutic areas, etc.[31] However, the potential use of isoxazole compounds to probe mtPTP-related diseases has not been reported. Although not directly comparable with activity against the mtPTP, piperazinylalkylisoxazole compounds have been reported as inhibitors of T-type Ca^{2+} channel blockers.[32] Regardless, the isoxazole compounds reported herein contain a phenyl ring at the 5-position of the isoxazole unit and an anilide functionality off the 3-position, and these features make the isoxazole compounds reported herein structurally unique to the above-mentioned piperazinylalkylisoxazole-containing compounds.

Isoxazole compound analogue synthesis

Generally, analogues of **1** were assembled by coupling the isoxazole-core-containing carboxylic acids **2** and anilines **3** using thionyl chloride and triethylamine in tetrahydrofuran (THF) (Scheme 1 A) to afford the corresponding isoxazole amides **4** in 20–80% yield. For some of these isoxazole amides, the corresponding carboxylic acid partners, as well as the aniline coupling partners, were commercially available. For the assembly of non-isoxazole-core-containing amides, a similar coupling strategy was used (Scheme 1 B).

For the isoxazole-containing or different heterocycle-containing carboxylic acids that were not commercially available, a three-step procedure was required for their assembly (Scheme 2). The acetophenone derivatives **8** were treated with dimethyl oxalate and sodium methoxide in diethyl ether for 24 h at room temperature to give the corresponding 1,3-diketones[33] **9** in 60–80% yield, which are present predominantly in the enol form, **9a**. At this point, depending on the desired heterocyclic motif, the enols **9a** were treated with hydroxylamine hydrochloride in methanol under reflux conditions to form the isoxazole[34] core **10a**, or, upon treatment with hydrazine hydrate in acetic acid, afforded the pyrazole core as a 1:1 mixture of regioisomers **10b**/**10b′**, whereas using methylhydrazine in methanol under reflux conditions afforded a 1:1 mixture of regioisomers of the methylpyrazoles **10c**/**10c′** in 40–90% overall yield. Subsequent saponification of the methyl esters in these compounds with sodium hydroxide in ethanol/THF (2:1) for 2 h at reflux provided the corresponding carboxylic acid intermediates **11a**, **11b**, **11b′**, **11c**, and **11c′** in 70–98% yields.

Structure–activity relationship optimization

Using CsA and GNX-865 as positive controls, SAR optimization was driven using three assays, namely: 1) mitochondrial swel-

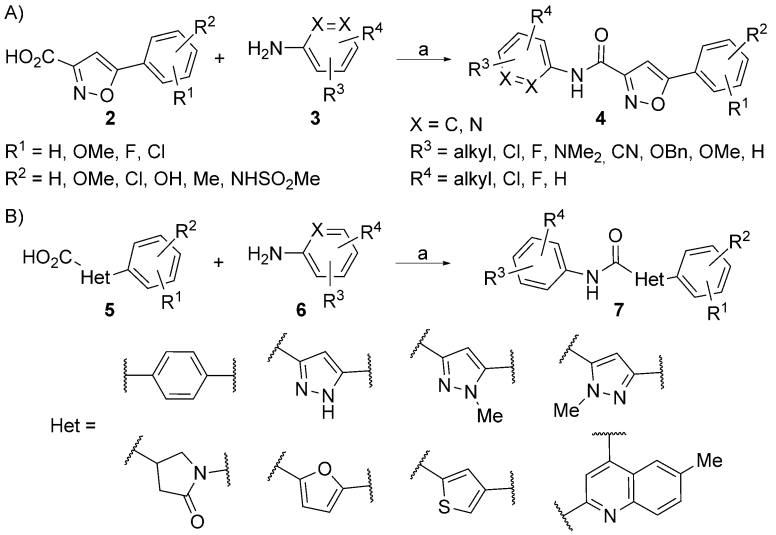

Scheme 1. Synthetic route for the assembly of isoxazole analogues. *Reagents and conditions*: a) $SOCl_2$, Et_3N, 65 °C→RT, THF, 20–80%.

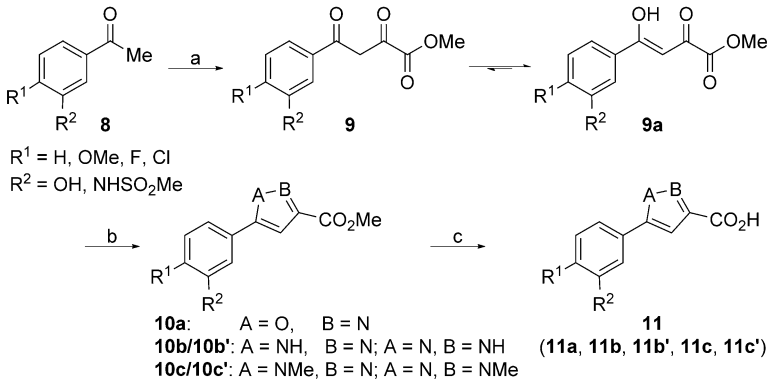

Scheme 2. Synthetic route for isoxazole carboxylic acid intermediates. *Reagents and conditions*: a) dimethyl oxalate, NaOMe, Et_2O, RT, 24 h, 60–80%; b) $NH_2OH{\cdot}HCl/NH_2{\text-}NH_2{\cdot}H_2O/MeNH{\text-}NH_2$, MeOH/AcOH, reflux, 1/18 h, 40–90%; c) NaOH, EtOH/THF (2:1), reflux, 2 h, 70–98%.

ling, which is an absorbance-based assay used to assess the concentration–response activity of mtPTP inhibitors; 2) Rh123 uptake, which is a fluorescence-based counter-screen assay performed to identify compounds that prevent mitochondrial swelling by interfering with IMM potential rather than blocking or binding to the mtPTP; and 3) the CRC test, which measures the amount of Ca^{2+} accumulated and retained by the mitochondria before the precipitous Ca^{2+} release marking opening of the mtPTP. The ratio between the amounts of Ca^{2+} required to trigger pore opening in the presence (CRC) versus absence of test compound (CRC_0), is a direct measure of the inhibitory effect on the mtPTP and is known as the CRC ratio (CRC/CRC_0). Guided by these three key assays, we explored structural modifications primarily around the western and the eastern aryl rings and the isoxazole central core (highlighted regions in Figure 2) to discover efficacious inhibitors.

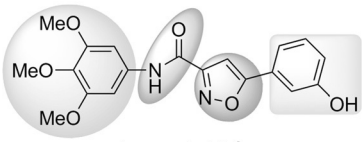

isoxazole hit **1**

mitochondrial swelling EC_{50}: <0.39 μM
Rh123 uptake EC_{50}: >100 μM
molecular weight: 370.3560 Da
exact mass: 370.1165 Da
molecular formula: $C_{19}H_{18}N_2O_6$
clog*P*: 2.211
tPSA: 98.61 $Å^2$

Figure 2. Regions of hit **1** earmarked for optimization.

With respect to SAR for the western aryl ring, it became evident that introduction of the 3-chlorophenyl moiety improved activity (Table 1, entry **14**) and migration of the chlorine atom or its replacement around the ring (entry **15** versus **16**) caused activity to decrease. Introducing 3,5-dichloro or 3-chloro-5-methyl substitution on the phenyl ring (entries **23** and **30**), as well as the 5-chloro-2-methyl, 5-chloro-2-cyano, 5-chloro-2-methoxy pattern on the phenyl ring (entries **29**, **25**, and **27**), which all have the 3-chlorophenyl moiety intact, resulted in considerable enhancement in activity. Interestingly, introducing the 2,6-dimethylphenyl moiety enhanced activity (entry **33**), which might suggest a role for sterics in perturbing the coplanarity of the 2,6-dimethylphenyl ring and the amide bond. Introducing a heteroatom in the phenyl ring (entry **31**) was tolerated with a modest loss of activity.

With respect to the eastern aryl ring, varying the position of the phenolic hydroxy group (Table 2, entries **38**–**43**), bioisosteric replacement of the hydroxy group with *N*-methylsulfonamide ($NHSO_2Me$; entries **44** and **45**), protection of the hydroxy group as methoxy (entry **37**), and deletion of the hydroxy group (entry **35**), resulted in diminished or no activity, indicating the importance of the 3-hydroxyphenyl moiety.

Having determined desirable substitution patterns on the eastern and western aryl rings, we explored the effect of additional substituents in the eastern aryl ring. To that end, we explored the effect of electron-withdrawing and electron-donating groups on the adjacent phenol group. Analogues containing the 3-hydroxy-4-methoxyphenyl moiety resulted in very-good-to-excellent activity (Table 3, entries **46**–**55**), particularly the 5-chloro-2-methylphenyl amalgamation (entry **46**), which resulted in single-digit picomolar activity in the mitochondrial swelling assay and a very high CRC ratio of 10 at 1.56 μM, whereas the 3-chloro-2-methylphenyl combination (entry **52**) showed similar potency of 28 pM activity in the mitochondrial swelling assay and a CRC ratio of 9.6 at 1.56 μM. Furthermore, the 5-chloro-2-methylpyridin-3-yl counterpart displayed 10 nM activity in the mitochondrial swelling assay and a CRC ratio of 10 (entry **54**). However, complete loss of activity was observed with the incorporation of 3,4-dimethoxyphenyl substitution in the eastern ring, reiterating the importance of the 3-hydroxyphenyl moiety for activity (entries **56** and **57**).

With respect to exploring the effect of electron-withdrawing groups by introducing a fluoro functionality adjacent to the phenolic hydroxy group, we obtained inhibitory activity analogous to that observed for the methoxy series, and, in some cases, even better activity (entries **58**–**67**). The 5-chloro-2-methylphenylanilino and 3-chloro-2-methylphenylanilino analogues demonstrated sub-nanomolar activity in the mitochondrial swelling assay and very high CRC ratios of 15 and 12, respectively, at 1.56 μM (entries **63** and **60**). The chloro-2-methylpyridin-3-yl aniline analogue displayed 16 nM activity in the mitochondrial swelling assay along with a CRC ratio of 9 (entry **66**). Similarly, insertion of a chloro functionality adjacent to the phenolic hydroxy group afforded analogues with good activity (entries **68**–**70**).

Finally, we studied modifications to the central core of the scaffold. Replacing the isoxazole core with phenyl (Table 4, entry **71**), 6-methylquinoline (entries **77** and **84**), and 5-oxopyrrolidine (entries **78** and **79**) rings attenuated the activity. Conversely, replacement with 1*H*-pyrazole or 1-methyl-1*H*-pyrazole conserved activity (entries **72**–**74**), whereas their regioisomers (entries **75** and **76**) were inactive. More surprising was the effect of introducing thiophene and furan rings (entries **80**, **81**, and **82**), as the resulting compounds showed activity in the Rh123 uptake assay, indicative of preventing mitochondrial swelling by interference with IMM potential rather than blocking or binding to the mtPTP.

Compound 60 is a key compound based on potency, selectivity, physicochemical properties, and efficiency indices

Overall, the SAR studies revealed a set of seven very potent analogues (Figure 3), with **46** having the lowest mitochondrial swelling activity ($EC_{50} = 7.6$ pM) and **63** having the highest CRC ratio of 15 at 1.56 μM. We identified four key compound analogues based on excellent inhibitory activities, CRC ratios, and physicochemical properties. These four analogues shared very promising physicochemical properties (Table 5) and desirable values for binding efficiency[35] metrics, such as ligand efficiency (LE) and lipophilic ligand efficiency (LLE). With respect to in vitro potency and efficacy, all four analogues were comparably

Table 1. Structure–activity relationships around the western aryl ring.

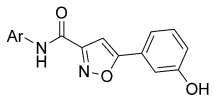

Entry	Ar	CRC/CRC$_0$[a,b]	EC$_{50}$ [μM][a] Mito[c]	Rh123[d]	Entry	Ar	CRC/CRC$_0$[a,b]	EC$_{50}$ [μM][a] Mito[c]	Rh123[d]
12		1.06 ± 0.04	> 50	> 100	**23**	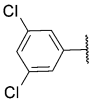	5.72 ± 0.25	0.190 ± 0.017	> 100
13	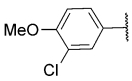	2.36 ± 0.14	0.189 ± 0.028	> 100	**24**	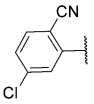	7.69 ± 0.61	0.0296 ± 0.0026	> 100
14		4.13 ± 0.17	0.0788 ± 0.0058	> 100	**25**	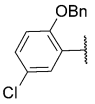	1.00 ± 0.00	17.6 ± 2.2	> 100
15	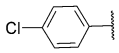	2.41 ± 0.05	0.887 ± 0.125	> 100	**26**		4.96 ± 0.31	0.0300 ± 0.0022	> 100
16		1.55 ± 0.11	12.7 ± 1.9	> 100	**27**	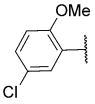	6.95 ± 1.15	0.0603 ± 0.0076	> 100
17	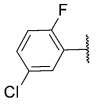	3.77 ± 0.10	0.172 ± 0.014	> 100	**28**	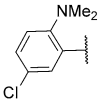	1.57 ± 0.14	1.61 ± 0.87	> 100
18	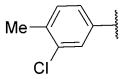	1.75 ± 0.13	7.06 ± 0.65	> 100	**29**	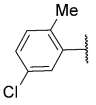	9.63 ± 0.29	0.0035 ± 0.0007	> 100
19		4.30 ± 0.26	0.0075 ± 0.0012	> 100	**30**	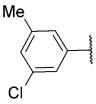	4.55 ± 0.45	0.0781 ± 0.0050	> 100
20		1.84 ± 0.07	12.5 ± 0.7	> 100	**31**	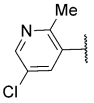	6.62 ± 0.69	0.0266 ± 0.0028	> 100
21	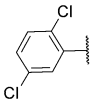	2.51 ± 0.30	1.52 ± 0.05	38.5 ± 4.0	**32**	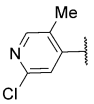	3.53 ± 0.37	0.100 ± 0.010	> 100
22		1.27 ± 0.11	42.7 ± 2.6	> 100	**33**	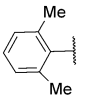	8.12 ± 0.59	0.0121 ± 0.0014	> 100
	CsA	4.46 ± 0.25	0.0953 ± 0.0029	> 100		GNX-865	4.53 ± 0.12	0.105 ± 0.007	> 100

[a] Data are the average ± SEM of $n \geq 3$ experiments. [b] At 1.56 μM. [c] Mitochondrial swelling. [d] Rhodamine 123 uptake.

matched; however, **60** and **63** were favored in terms of slightly decreased topological polar surface area and the number of hydrogen bond acceptors. In addition, the measured aqueous solubility for compound **60** was 16 μM in PBS at pH 7.4, which was the best of the four key analogues. In light of its promising in vitro potency, selectivity, and physicochemical properties, compound **60** was prioritized for more extensive biological characterization.

Profiling of compound 60 in Eurofins LeadProfilingScreen and for in vitro drug metabolism and pharmacokinetic properties

Compound **60** was profiled against a panel of 68 G-protein-coupled receptors (GPCRs), ion channels, and transporters. At a concentration of 10 μM, 79% inhibition of human norepinephrine transporter (NET) and 51% inhibition of adenosine A_3 were observed, whereas inhibition of the other 66 targets in the panel was ≤43%.[36] Moreover, the desired activity of compound **60** in the swelling assay is achieved at >1000-fold

Table 2. Structure–activity relationships around the eastern aryl ring.

Entry	Structure	CRC/CRC$_0$[a,b]	EC$_{50}$ [μM][a] Mito[c]	Rh123[d]
34	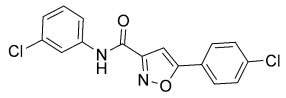	1.00 ± 0.00	> 50	> 100
35	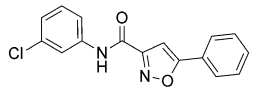	1.00 ± 0.00	> 50	> 100
36	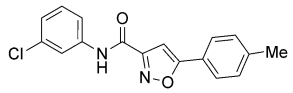	1.00 ± 0.00	> 50	> 100
37	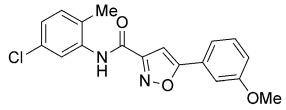	1.03 ± 0.08	44.6 ± 3.0	> 100
38	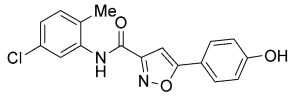	1.00 ± 0.00	> 50	> 100
39	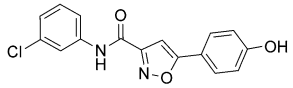	2.10 ± 0.20	2.21 ± 0.17	> 100
40	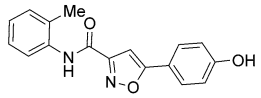	1.46 ± 0.15	2.45 ± 0.15	> 100
41	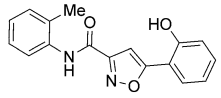	1.24 ± 0.09	> 50	> 100
42	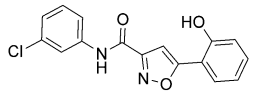	1.00 ± 0.00	> 50	> 100
43	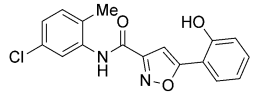	1.25 ± 0.09	6.05 ± 0.75	> 100
44	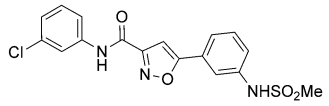	0.98 ± 0.02	> 50	> 100
45	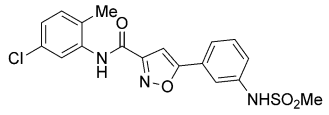	1.02 ± 0.02	> 50	> 100

[a] Data are the average ± SEM of $n \geq 3$ experiments. [b] At 1.56 μM. [c] Mitochondrial swelling. [d] Rhodamine 123 uptake.

lower concentration than the counter-screen activity against the NET and adenosine A_3 targets.

Compound **60** was submitted for in vitro drug metabolism and pharmacokinetic profiling to establish a baseline against which future analogues could be compared (Table 6). Compound **60** demonstrated acceptable human plasma protein binding and very high binding for mouse plasma proteins. Assessment of in vitro metabolism revealed a very good half-life in human plasma, whereas a poor half-life was observed in mouse plasma. Similarly, greater compound stability was observed in human liver microsomes, relative to the stability observed in mouse liver microsomes. Clearly, there is room for improvement for an optimized lead compound compared with compound **60**.

Inhibitory effect of compound 60 on Ca^{2+}-induced mtPTP opening

Elevated levels of matrix Ca^{2+} concentration and oxidative stress sensitize the mtPTP to open, resulting in an increased permeability of the otherwise impermeant IMM to ions and solutes up to ~1500 Da in size. In vitro mitochondrial volume changes can be followed spectrophotometrically as a decrease in absorbance at λ 540 nm. Consequently, we tested mtPTP opening in isolated mouse liver mitochondria, induced by a 50 μM Ca^{2+} load (Figure 4A, trace a) which was abolished in the presence of compound **60** at 1.56 μM, (Figure 4A, trace b). A full concentration–response assessment, ranging from 18.6 pM to 1.56 μM, revealed a mitochondrial swelling EC$_{50}$ value of 0.89 ± 1.42 nM (Figure 4B, trace a), which is two orders of magnitude more potent than that of CsA or GNX-865 (Table 1). Moreover, we confirmed that the lack of mitochondrial swelling in the presence of the inhibitors was due to mtPTP desensitization, and does not decrease the IMM potential (Figure 4B, trace b).

Compound 60 and CsA likely act on different biological targets

In the following assays, we used isolated mouse liver mitochondria as the test material because they are easily prepared and give consistent and reproducible results. Ample literature indicates that these mitochondria respond to pore agonists and inhibitors as human mitochondria respond.[3a] A suspension of mouse liver mitochondria supplemented with the membrane-impermeant fluorescent dye Calcium Green-5N at 0.5 μM was loaded with a train of 20 μM Ca^{2+} pulses until the threshold was reached and precipitous Ca^{2+} release was registered, marking opening of the mtPTP (e.g., Figure 4C). The presence of 1.56 μM **60** raised the Ca^{2+} load required for mtPTP opening from 80 to ~960 nmol(mg protein)$^{-1}$ (Figure 4C traces a and c, respectively), which was further increased by augmenting the concentration of **60**, eventually culminating in the compound-to-solvent CRC ratio of 15 (Figure 4D, trace a). Based on our findings that the maximum CRC ratios of isolated mouse liver mitochondria treated with **60** are ~3-fold higher than those treated with CsA (Figure 4C, compare traces c and a, and traces b and a), we suspected that our inhibitors and CsA act on different biological targets. To address this, we treated mitochondria with 2 μM CsA together with various concentrations of **60** and performed the CRC test. We found that the two compounds' effects are synergistic at

Table 3. Structure–activity relationships around the eastern aryl ring: effect of methoxy, fluoro, and chloro group substitution.

Entry	Structure	CRC/CRC$_0$[a,b]	EC$_{50}$ [μM][a] Mito[c]	Rh123[d]	Entry	Structure	CRC/CRC$_0$[a,b]	EC$_{50}$ [μM][a] Mito[c]	Rh123[d]
46	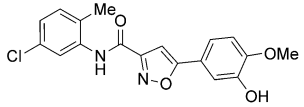	10.02 ± 0.34	0.00000756 ± 0.00000122	> 100	**58**	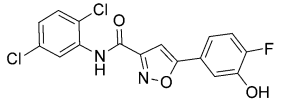	6.50 ± 0.77	0.0661 ± 0.0032	> 100
47	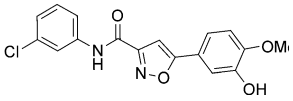	3.83 ± 0.12	0.0348 ± 0.0042	> 100	**59**	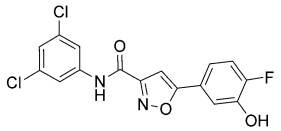	6.41 ± 1.19	0.0756 ± 0.0092	> 100
48	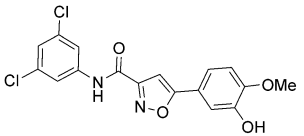	1.71 ± 0.11	0.277 ± 0.001	> 100	**60**	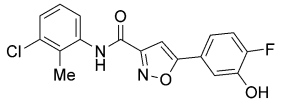	12.14 ± 0.55	0.000890 ± 0.000141	> 100
49	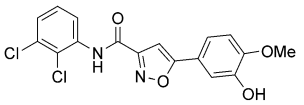	5.21 ± 0.50	0.108 ± 0.010	> 100	**61**	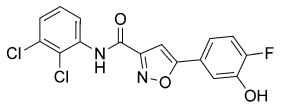	6.02 ± 0.78	0.0554 ± 0.0041	> 100
50	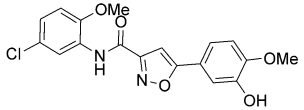	6.62 ± 0.84	0.0971 ± 0.0034	> 100	**62**	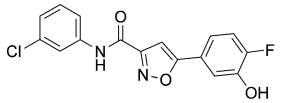	6.36 ± 0.66	0.0133 ± 0.0020	> 100
51	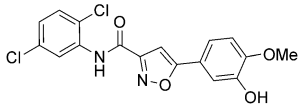	4.34 ± 0.53	0.146 ± 0.011	> 100	**63**	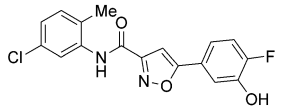	15.21 ± 1.26	0.000134 ± 0.000016	> 100
52	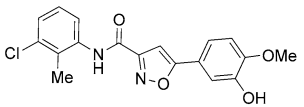	9.59 ± 0.85	0.0000283 ± 0.0000048	> 100	**64**	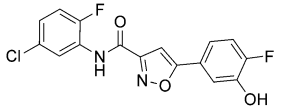	7.63 ± 0.64	0.00905 ± 0.00141	> 100
53	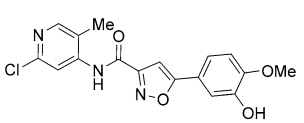	2.80 ± 0.18	0.365 ± 0.048	> 100	**65**	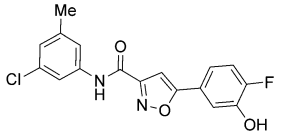	3.35 ± 0.28	0.819 ± 0.059	> 100
54	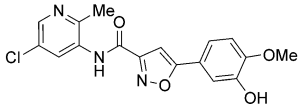	10.10 ± 1.14	0.0105 ± 0.0011	> 100	**66**	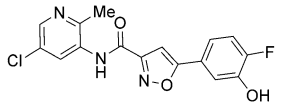	9.12 ± 0.88	0.0155 ± 0.0018	> 100
55	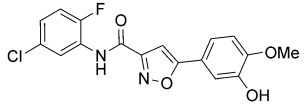	2.90 ± 0.15	0.217 ± 0.052	> 100	**67**	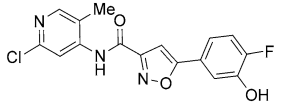	2.01 ± 0.23	2.19 ± 0.15	> 100

Table 3. (Continued)

Entry	Structure	CRC/CRC_0[a,b]	EC_{50} [μM][a] Mito[c]	Rh123[d]
56	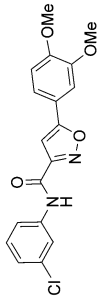	1.00 ± 0.00	> 50	> 100
57	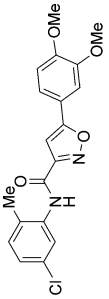	1.00 ± 0.00	> 50	> 100
68	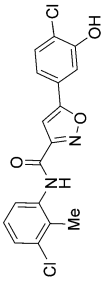	8.22 ± 0.58	0.000180 ± 0.000042	> 100
69	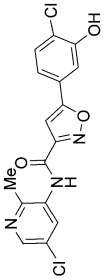	6.91 ± 0.47	0.00134 ± 0.00026	> 100
70	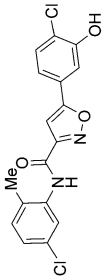	6.21 ± 0.66	0.00216 ± 0.00045	> 100

[a] Data are the average ± SEM of $n \geq 3$ experiments. [b] At 1.56 μM. [c] Mitochondrial swelling. [d] Rhodamine 123 uptake.

all tested concentrations of **60** (Figure 4C,D), indicating the target of diarylisoxazole-3-carboxamides is likely not CyPD.

Compound 60 inhibits human mtPTP

Given that our mtPTP inhibitors were identified and optimized using murine mitochondria, and that species-specific regulation of the mtPTP has been demonstrated,[18b,37] we tested whether human mtPTP is also affected by **60**. The inhibitory effect of **60** on human mitochondria was initially confirmed by the increased CRC ratios of permeabilized HeLa cells upon treatment with increasing concentrations of **60** (Figure 4F). Moreover, we treated intact HeLa cells with 1.56 μM **60** or DMSO for 30 min and washed them to eliminate excess **60** by centrifugation. Cells were then permeabilized with digitonin, and the CRC was assessed. As shown in Figure 4E, we observed that **60** is effective following treatment of intact human cells (compare traces a and c), indicating that it was able to permeate the plasma membrane and reach its mitochondrial target, thus desensitizing mtPTP activation to the same extent as DMSO-treated cells (trace b).

Compound 60 protects against chemical activation of mtPTP

We next investigated whether **60** is protective against known chemical activators of the mtPTP that result in oxidative stress and trigger pore opening. We pretreated isolated mouse liver mitochondria with 10 μM Ca^{2+}, an amount insufficient to induce mtPTP opening per se (Figure 5 traces a), and challenged them with reagents that react with two distinct classes of redox-sensitive thiols and increase the mtPTP sensitivity to Ca^{2+}: 1) PhAsO (Figure 5A) and diamide (Figure 5B), which react with matrix thiols;[38] and 2) $Cu(OP)_2$ and NEM (Figure 5C,D, respectively), which react with intermembrane space exposed thiol groups.[39] In all cases, the mtPTP transition, from closed to open conformation, was delayed by CsA at 1.56 μM and was prevented by compound **60** at the same concentration, as measured by the lack of mitochondrial swelling (Figure 5 traces c and d, respectively). Therefore, the isoxazole inhibitors prevented mtPTP opening irrespective of changes in calcium flux and stimuli that would induce pore opening.

Compound 60 shows no effect on ATP synthesis and HeLa cell proliferation

Because it was recently suggested that the mtPTP is formed by a unique conformation of F-ATP synthase dimers,[18,37b] we investigated whether apart from preventing mtPTP formation, compound **60** also affects ATP synthesis, a potentially untoward side effect. Thus, we measured mitochondrial respiration both in isolated mouse liver mitochondria and in intact HeLa cells in the presence or absence of the inhibitor. No statistically significant differences in respiratory control ratios (Figure 6B), or FCCP-stimulated and oligomycin-insensitive respiration were observed in both isolated mouse liver mitochondria (Figure 6A) and HeLa cells (Figure 6C), demonstrating that the diarylisoxazole-3-carboxamides do not affect the respiratory chain

Table 4. Replacement of the isoxazole ring.

Entry	Structure	CRC/CRC$_0$[a,b]	EC$_{50}$ [μM][a] Mito[c]	Rh123[d]	Entry	Structure	CRC/CRC$_0$[a,b]	EC$_{50}$ [μM][a] Mito[c]	Rh123[d]
71	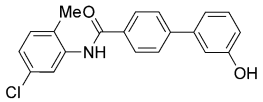	1.47 ± 0.12	4.71 ± 0.35	> 100	**78**	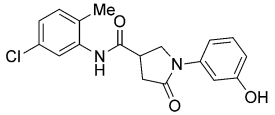	1.09 ± 0.03	13.9 ± 0.8	> 100
72	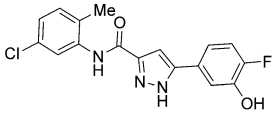	10.92 ± 0.74	0.0014 ± 0.0002	30.4 ± 5.5	**79**	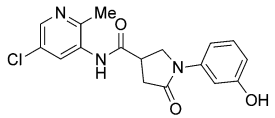	1.02 ± 0.02	> 50	> 100
73	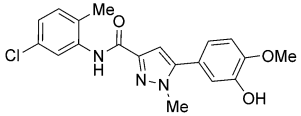	7.51 ± 0.47	0.0024 ± 0.0004	> 100	**80**	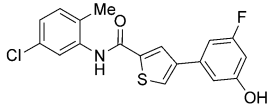	1.21 ± 0.07	6.43 ± 1.11	5.47 ± 0.29
74	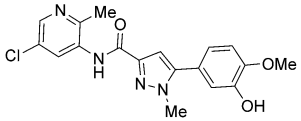	2.26 ± 0.15	0.0211 ± 0.0020	> 100	**81**	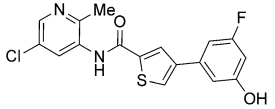	1.04 ± 0.02	34.4 ± 3.17	21.0 ± 2.2
75	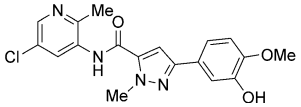	1.00 ± 0.00	> 50	> 100	**82**	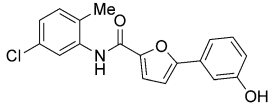	0.98 ± 0.02	35.2 ± 2.3	39.6 ± 3.0
76	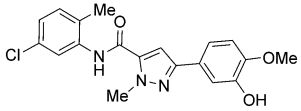	1.00 ± 0.00	> 50	> 100	**83**	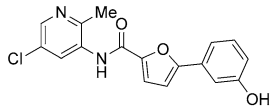	0.93 ± 0.06	> 50	> 100
77	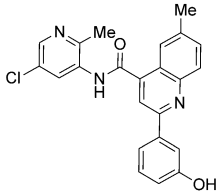	1.00 ± 0.00	> 50	> 100	**84**	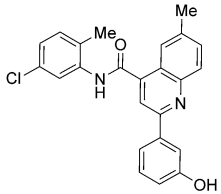	1.00 ± 0.00	> 50	> 100

[a] Data are the average ± SEM of $n \geq 3$ experiments. [b] At 1.56 μM. [c] Mitochondrial swelling. [d] Rhodamine 123 uptake.

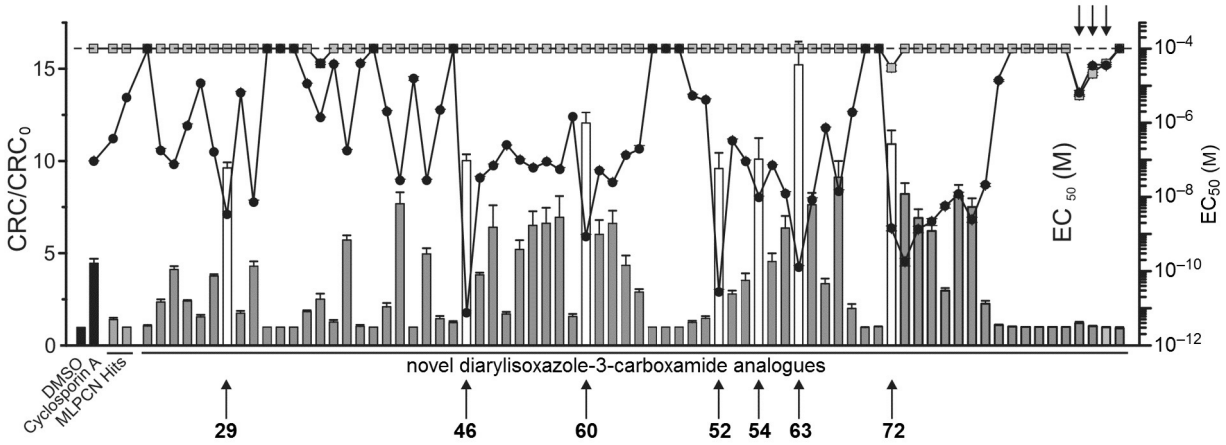

Figure 3. SAR overview. CRC ratios at 1.56 μM compound concentration (bars), swelling (circles), and Rh123 uptake (squares). EC_{50} values are for isolated mouse liver mitochondria. Data are the average ± SEM of $n \geq 3$ experiments. Values equal to those on the dashed line represent $EC_{50} > 50$ μM and > 100 μM for the swelling and Rh123 uptake assays, respectively.

Table 5. Potency, selectivity, physicochemical properties, and efficiency indices for key compounds.

Parameter	HTS hit **1**	Compd **46**	Compd **54**	Compd **60**	Compd **63**
CRC/CRC_0[a]	1.18 ± 0.06	10.0 ± 0.3	10.1 ± 1.1	12.1 ± 0.6	15.2 ± 1.3
Mito EC_{50} [μM][b]	< 0.39	0.00000756 ± 0.00000122	0.0105 ± 0.0010	0.000890 ± 0.000141	0.000134 ± 0.000016
Rh123 EC_{50} [μM][c]	> 100	> 100	> 100	> 100	> 100
HeLa CC_{50} [μM][d]	ND[m]	> 50	> 50	39.5 ± 4.65	44.5 ± 1.67
M_r [Da][e]	370.3	358.7	359.7	346.7	346.7
tPSA [Å^2][e,f]	98.6	80.1	92.5	70.9	70.9
clog P[e]	2.2	3.4	2.3	3.7	3.7
HBA[g,h]	7	5	6	4	4
HBD[g,i]	2	2	3	2	2
Heavy atoms[j]	27	25	25	24	24
LE[k]	0.32	0.60	0.43	0.51	0.56
LLE[l]	4.2	7.6	5.5	5.2	6.1

[a] At 1.56 μM. [b] Mitochondrial swelling. [c] Rhodamine 123 uptake. [d] HeLa cell cytotoxicity. [e] Data were generated using CambridgeSoft ChemBioDraw version 12. [f] Topological polar surface area. [g] Data were calculated using SYBYL 8.0, 2010, Tripos Associates, St. Louis, MO (USA). [h] Hydrogen bond acceptors. [i] Hydrogen bond donors. [j] Data were calculated using Marvin 15.3.23.0, 2015, ChemAxon. [k] Ligand efficiency. [l] Lipophilic ligand efficiency. [m] Not determined.

Table 6. Summary of in vitro ADME data for compound **60**.

Parameter[a]	Compd **60**
Aqueous solubility [μM] (PBS, pH 7.4)	16.1
Protein binding {recovery} [%] (human; mouse)	89 {76}; > 99 {0}
Plasma stability $t_{1/2}$ [min] (human; mouse)[b]	> 120; < 30
CL_{int} HLM [μL min^{-1} mg^{-1}][b,c]; $t_{1/2}$ [min][b]	< 115.5; > 60
CL_{int} MLM [μL min^{-1} mg^{-1}][b,d]; $t_{1/2}$ [min][b]	> 462; < 15

[a] Data collected at Cerep/Eurofins Panlabs. [b] The remaining compound percentage at multiple time points is reported in the Supporting Information. [c] Intrinsic clearance, human liver microsomes. [d] Intrinsic clearance, mouse liver microsomes.

complexes or inherent function of F-ATP synthase. Indeed, compound **60** was not cytotoxic up to a concentration of 12.50 μM (CC_{50} = 39.5 ± 4.65 μM; Figure 6D) as confirmed by the similar number of viable HeLa cells after treatment for 24 h. Note that as an additional precaution, the plasma membrane multidrug resistance pump inhibitor CsH (which does not inhibit the PTP)[40] (Figure 6D) or verapamil[41] (data not shown) were added in these experiments to ensure that **60** is not extruded from the cells. Similar results were observed following treatment of HEK293 cells and murine embryonic fibroblasts with **60** (data not shown).

Compound 60 shows therapeutic potential in a validated vertebrate model of mtPTP-based disease

As noted above in the Introduction, activation of the mtPTP has been implicated in some of the most challenging human disorders. Indeed, our true appreciation of the extent of mtPTP activation in human diseases was only fully developed through the creation of mice lacking CyPD and performing tests in murine models of these disorders. Among these are muscular dystrophies due to the absence of the extracellular matrix protein ColVI. ColVI is an essential component of myofiber extracellular matrix; mutations in ColVI result in two major human

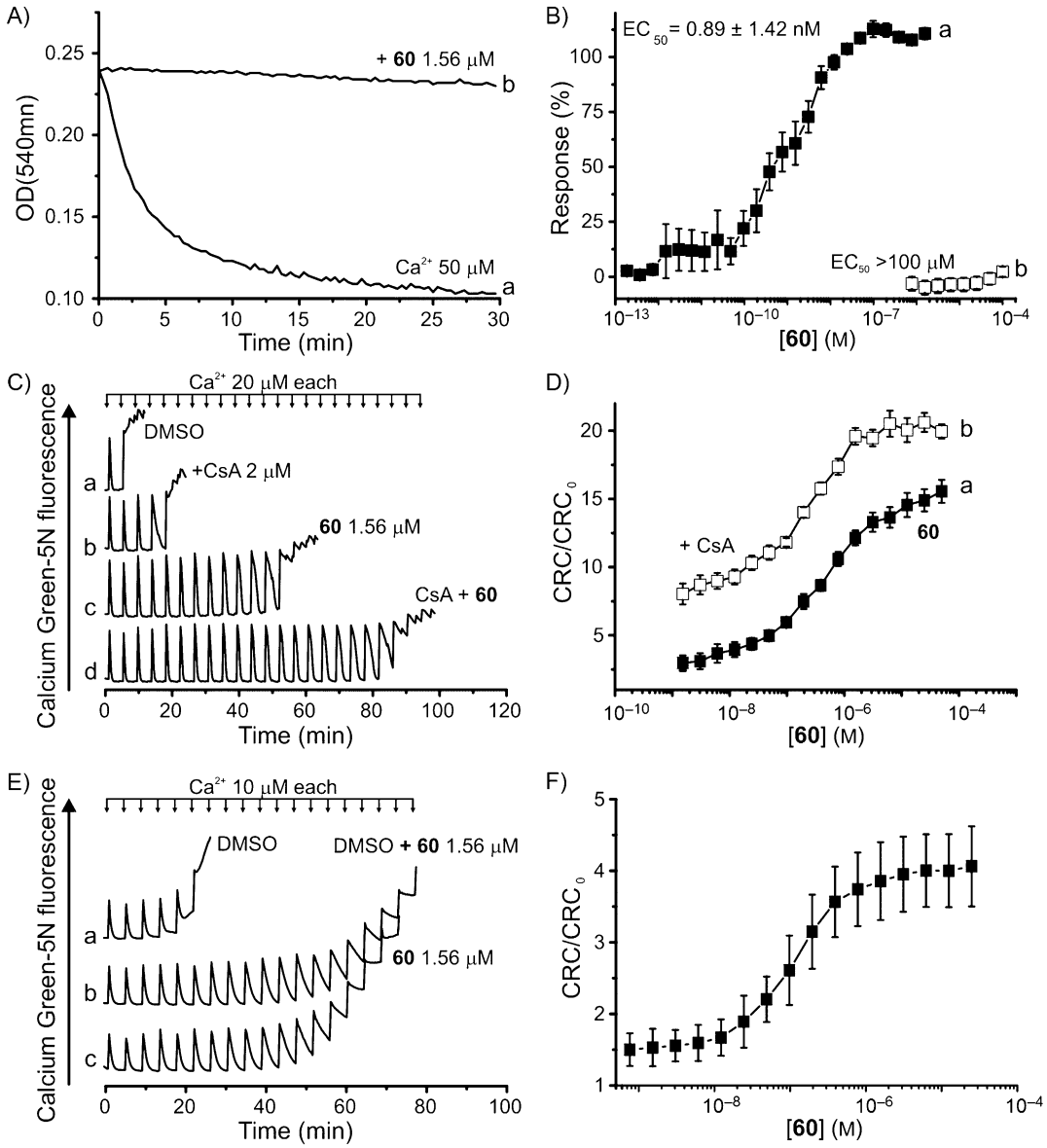

Figure 4. Effect of **60** on Ca^{2+}-induced mtPTP. A) Mitochondrial swelling was induced with 50 μM Ca^{2+}, which was prevented with **60**. B) Concentration–response of experiment described in panel A (■) and interference with Rh123 uptake (□). C) Representative CRC of DMSO-, CsA-, **60**-, and CsA + **60**-treated mitochondria; D) Concentration–response of **60** (■) and CsA (2 μM) + **60** (□)-to-solvent CRC ratios; assays were performed on isolated mouse liver mitochondria (0.25 mg mL^{-1}). E) Representative CRCs of HeLa cells treated with DMSO (trace a) or **60** (1.56 μM; trace c) before cell permeabilization with digitonin; trace b: cells were treated as in trace a and CRC was performed in the presence of **60** (1.56 μM). F) **60**-to-solvent CRC ratios of permeabilized HeLa cells (0.8×10^6 per condition). Data are the average ± SEM of $n \geq 5$ experiments.

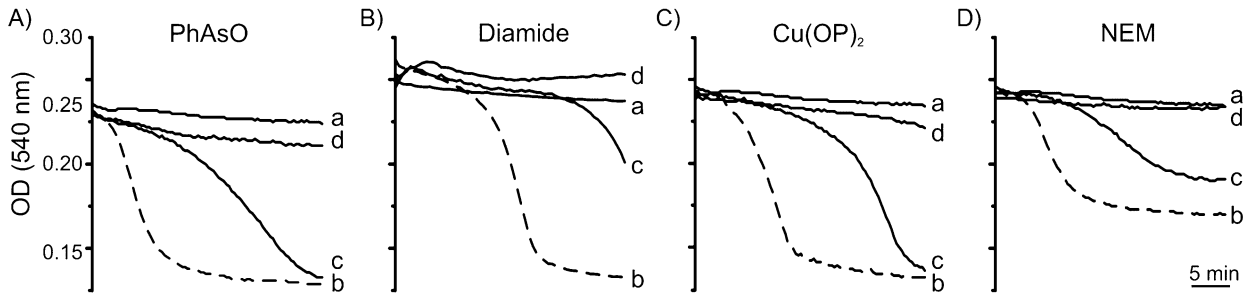

Figure 5. Effect of **60** on chemical activation of the mtPTP. Suspension of isolated mouse liver mitochondria (0.25 mg mL^{-1}) were supplemented with 10 μM Ca^{2+} only (traces a); 10 μM Ca^{2+} and A) 7 μM PhAsO, B) 2 mM diamide, C) 7 μM $Cu(OP)_2$, or D) 2 mM NEM (traces b–d). In traces c and d, 1.56 μM CsA or **60**, respectively, were also present. Traces are representative of four separate experiments.

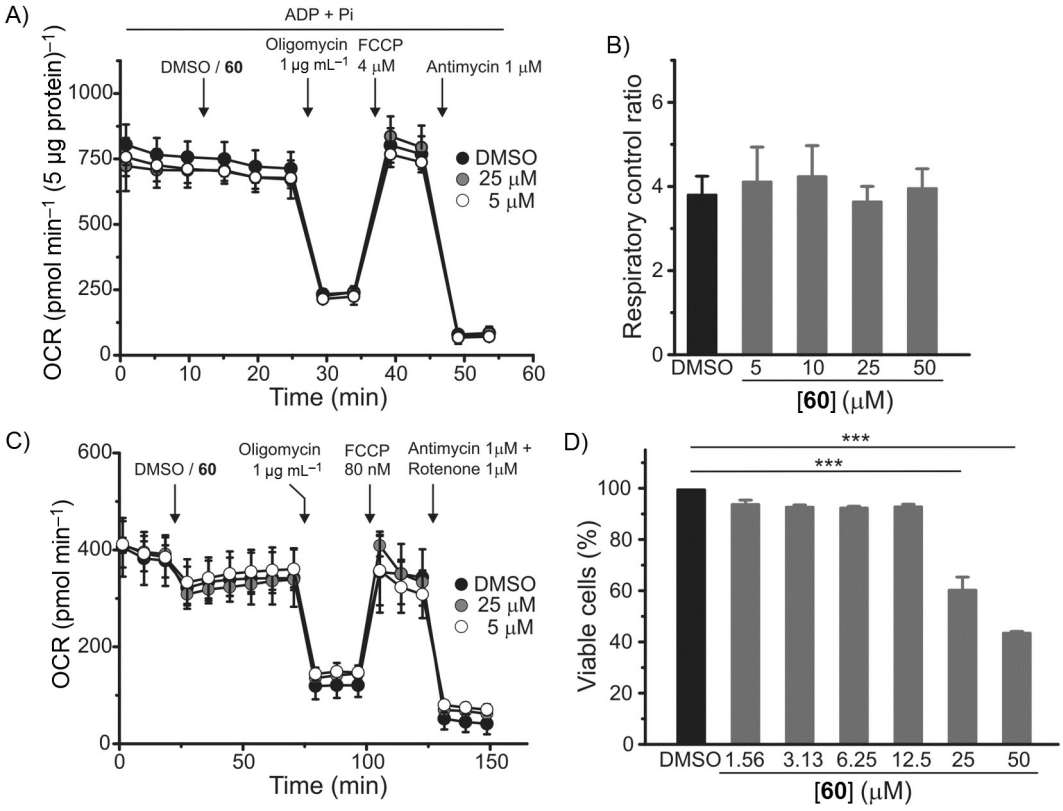

Figure 6. Effect of **60** on oxygen consumption rate (OCR) and HeLa cell proliferation. A) OCR of ADP + Pi-stimulated isolated mouse liver mitochondria. B) Ratios of OCR before-to-after addition of oligomycin. C) OCR of HeLa cells. D) Interference with HeLa cell proliferation after 24 h treatment with the indicated concentration of compound **60**. In panels C and D, the multidrug resistance inhibitor CsH (2 μg mL^{-1}) was also present. Similar results were obtained with 20 μM verapamil. A), C) Data are the average ± SD of a representative experiment performed four separate times. B), D) Data are the average ± SEM of four and five experiments, respectively; ***$p < 0.001$ as assessed by *t*-test.

diseases: Ullrich congenital muscular dystrophy (UCMD) and Bethlem myopathy (BM).[42] Mouse models of UCMD have been created through knock-out of the murine *Col6a1* gene, but, in contrast to UCMD patients, homozygous recessive animals exhibit very mild clinical myopathy.[43] However, in both humans and mice, assessment of mitochondrial characteristics amply documented that inappropriate mtPTP activity plays a key role in disease pathogenesis.[43b,44] Consistent with this idea, modification of the mtPTP, either pharmacologically in humans and in mice (with CsA and non-immunosuppressive derivatives such as Debio025 or NIM811),[8b,25b,28b,45] or elimination of the mouse gene encoding CyPD,[46] was found to improve mitochondrial changes and to decrease myofiber cell death. A more robust model of UCMD has been generated in zebrafish by the injection of antisense morpholino oligonucleotides directed to the exon 9 splicing region of the orthologous *ColVIa* gene.[28] This treatment results in an in-frame deletion paralleling common mutations in UCMD.[47] Severe myopathy, motor deficits, and dramatic ultrastructural defects are present in morpholino-injected animals that successfully recapitulate the clinical severity of human UCMD.[28] Furthermore, treatment with NIM811[28b] reversed many of these defects. Consequently, we used the zebrafish ColVI myopathic model as a convenient, powerful, and easily assayed in vivo system to validate the therapeutic potential of the most potent diarylisoxazole-3-carboxamide mtPTP inhibitors outlined here.

Zebrafish embryos were injected at the 1–2-cell stage with morpholinos designed to mimic *ColVIa* exon 9 splicing defects common in UCMD.[47] Control morpholinos represent sequences not found in the zebrafish genome. Exon 9 morphant-treated embryos were then assayed using validated motor assays for defective motor function and muscle defects at 24 and 48 h post-fertilization (hpf). Motor function was assessed by spontaneous coiling events, reflecting twisted myofibrils, and "touch-evoked escape response".[45a] This assay measures the ability of embryos to "escape" after touching them with a small tip. The responses of embryos in this assay were subdivided into four groups according to their ability to escape: normal embryos with unaltered ability to swim, embryos with minor motility disruptions, embryos showing only spontaneous coiling events around the body axis without the ability to escape, and paralyzed embryos with no motility. As reflected in Figure 7 A,B, 87% of embryos injected with exon 9 morpholino showed severe motor impairments relative to control embryos. In contrast, exon 9 morphants treated with **60**, simply added to the fish water, showed a dramatic improvement in motor function as demonstrated with spontaneous coiling events (Figure 7 A) or touch-evoked response (Figure 7 B).

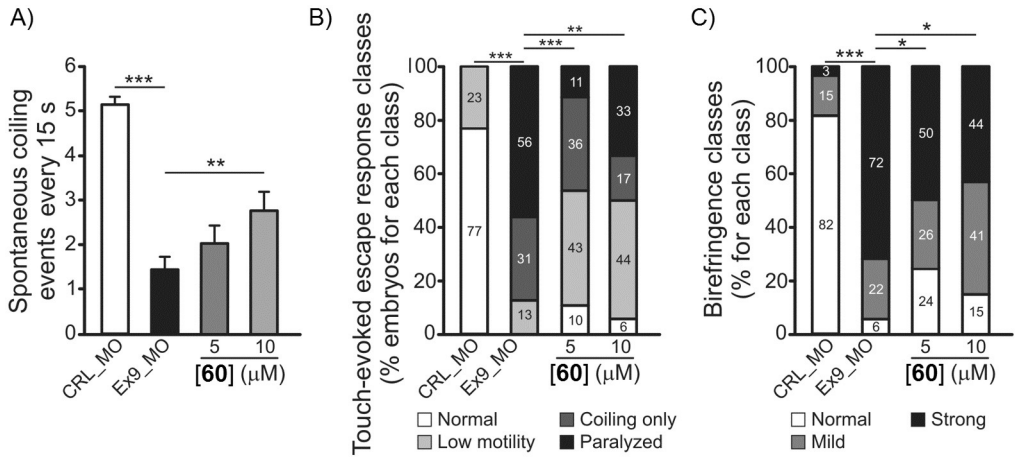

Figure 7. Effect of **60** on defects present in exon 9 *col6a1* morphant zebrafish. A) Coiling events were recorded at 24 hpf in control (CRL_MO) and exon 9 morphant (Ex9_MO) embryos in the presence of the indicated concentrations of **60** added at 21 hpf. Data are the mean ± SEM of at least five independent experiments ($n = 52$ for each condition); $^{**}p < 0.01$, $^{***}p < 0.001$ as determined by one-way ANOVA test with Bonferroni correction. B) In the presence of the indicated concentrations of **60** added at 21 hpf, response evoked by touching embryos at 24 hpf with a pipette tip were recorded. Embryos ($n = 35$ for each condition) were assigned to four groups based on their escape response: normal, low motility defects, spontaneous coiling events only, and complete paralysis. Results are reported as the percentage of total embryos analyzed for each group. Comparison between groups at different conditions was made using χ^2 test and one-way ANOVA with Bonferroni correction; $^{**}p < 0.01$, $^{***}p < 0.001$. C) Bar graphs report the percentage of birefringence classes at 48 hpf after treatment with compound **60** added at 21 hpf, showing normal birefringence, mild myopathic phenotype, and strong myopathic phenotype, as indicated. The total number of embryos used was $n = 35$ for each condition; $^{*}p < 0.05$, $^{***}p < 0.001$, as determined by χ^2 test and one-way ANOVA with Bonferroni correction.

To assess structural muscle organization, muscle birefringence was evaluated at 48 hpf. This technique evaluates muscle structural defects in zebrafish models of muscular dystrophy.[48] Muscle birefringence was analyzed by taking advantage of muscle fiber anisotropy. As can be seen in Figure 7C, exon 9 morphants exhibited severe muscle defects relative to controls, and these defects were largely ameliorated following treatment with **60**. Indeed, total birefringence scores demonstrated that treatment with **60** generated significant recovery of muscle defects (ANOVA, $p < 0.05$).

Conclusions

In summary, a high-throughput screening and SAR optimization effort to identify mtPTP inhibitors has resulted in isoxazole compounds whose structure, activity, and properties were optimized to yield highly valuable probes with picomolar inhibitory activity and potential for further development as treatments for a variety mtPTP-related diseases. We confirmed that the isoxazole inhibitors do not interfere with the IMM potential and are protective against known chemical activators of the mtPTP that induce oxidative stress and trigger pore opening. Moreover, the key analogues demonstrated activity synergistic with CsA, suggesting that the target is not CyPD. We noted that the isoxazole inhibitors do not affect the inherent function of F-ATP synthase or impact the cell viability at effective concentrations. Detailed studies to identify the biological mechanism of action for these compounds are underway. Finally, we validated the therapeutic potential and in vivo efficacy of the most efficacious analogue, **60**, in the zebrafish ColVI myopathic model. Future lead optimization work will focus on improving the in vitro and in vivo pharmacokinetic properties for the compound series and on evaluating the resulting analogues for activity in a variety of mtPTP-related disease models.

Experimental Section

Chemistry

General procedures. All solvents and reagents were used as received from commercial suppliers, unless noted otherwise. ^{1}H and ^{13}C NMR spectra were recorded on a Bruker AM 400 spectrometer (operating at 400 and 101 MHz, respectively) or a Bruker AVIII spectrometer (operating at 500 and 126 MHz, respectively) in $CDCl_3$ with 0.03% TMS as an internal standard. Chemical shifts (δ) are reported in parts per million (ppm), and coupling constants (J) are in Hertz (Hz). Spin multiplicities are reported as s = singlet, d = doublet, t = triplet, q = quartet, dd = doublet of doublet, ddd = doublet of doublet of doublet, dt = doublet of triplet, td = triplet of doublet, and m = multiplet. Microwave reactions were carried out using a Biotage Initiator Classic. Column chromatography separations were performed using the Teledyne Isco CombiFlash R_f using RediSep R_f silica gel columns. Analytical RPLC involved an Agilent 1200 RRLC system with UV detection (Agilent 1200 DAD SL) and mass detection (Agilent 6224 TOF). Analytical method conditions included a Waters Aquity BEH C_{18} column (2.1 × 50 mm, 1.7 μm) and elution with a linear gradient of 5% CH_3CN in buffered aqueous ammonium formate (pH 9.8) to 100% CH_3CN at a flow rate of 0.4 mL min^{-1}. Automated preparative RP HPLC purification was performed using an Agilent 1200 Mass-Directed Fractionation system (Prep Pump G1361 with gradient extension, make-up pump G1311A, pH modification pump G1311A, HTS PAL autosampler, UV-DAD detection G1315D, fraction collector G1364B, and Agilent 6120 quadrupole spectrometer G6120A). Preparative chromatography conditions included a Waters X-Bridge C_{18} column (19 × 150 mm, 5 μm, with 19 × 10 mm guard column), elution with a H_2O/CH_3CN gradient, which increased to 20% CH_3CN content

over 4 min at a flow rate of 20 mL min^{-1} (modified to pH 9.8 by the addition of NH_4OH by auxiliary pump), and sample dilution in DMSO. The preparative gradient, triggering thresholds, and UV wavelength were selected according to the analytical RP HPLC analysis of each crude sample. Compound purity was measured on the basis of peak integration (area under the curve) from UV/Vis absorbance at λ 214 nm, and compound identity was determined on the basis of mass spectral and NMR analyses. All compounds had >95% purity as determined by the HPLC methods described above.

General synthesis procedure: To a solution of isoxazole carboxylic acid (0.390 mmol, 1 equiv) in dry THF (1.5 mL) in a 4-dram vial was added $SOCl_2$ (0.558 mmol, 1.43 equiv), and the resulting solution was stirred at reflux for 0.5 h. After cooling the reaction mixture to 35 °C, a solution of 5-chloro-2-methylaniline (0.390 mmol, 1 equiv) and Et_3N (1.560 mmol, 4 equiv) in dry THF (1 mL) was added dropwise. After stirring at RT for 2 h the reaction mixture was quenched by the addition of 1 N HCl and extracted with EtOAc (3×2 mL). The combined organic layer was dried over anhydrous Na_2SO_4, filtered, and concentrated. The residue was analyzed and purified according to the analytical- and preparative-scale RP HPLC methods.

***N*-(5-Chloro-2-methylphenyl)-5-(3-hydroxy-4-methoxyphenyl)isoxazole-3-carboxamide (46)**: This compound was prepared following the general procedure using 5-(3-hydroxy-4-methoxyphenyl)isoxazole-3-carboxylic acid (11 mg, 0.047 mmol) and 5-chloro-2-methylaniline (7 mg, 0.047 mmol). Isolated compound **46** as an off-white powder (8 mg, 47%): mp: 186–192 °C (dec.); ^{1}H NMR (400 MHz, [D$_6$]DMSO): δ = 10.28 (s, 1H), 9.49 (s, 1H), 7.52 (d, J = 2.2 Hz, 1H), 7.41 (dd, J = 8.4, 2.2 Hz, 1H), 7.36–7.29 (m, 2H), 7.30–7.22 (m, 2H), 7.09 (d, J = 8.5 Hz, 1H), 3.85 (s, 3H), 2.24 ppm (s, 3H); ^{13}C NMR (101 MHz, [D$_6$]DMSO): δ = 170.9, 159.2, 157.4, 150.0, 146.9, 136.5, 132.1, 131.8, 129.8, 126.0, 125.5, 117.8, 112.5, 98.4, 55.7, 17.2 ppm; HRMS (ESI TOF) m/z: $[M+H]^+$ calcd for $C_{18}H_{16}ClN_2O_4$: 359.0793, found: 359.0789.

***N*-(5-Chloro-2-methylpyridin-3-yl)-5-(3-hydroxy-4-methoxyphenyl)isoxazole-3-carboxamide (54)**: This compound was prepared following the general procedure using 5-(3-hydroxy-4-methoxyphenyl)isoxazole-3-carboxylic acid (25 mg, 0.106 mmol) and 5-chloro-2-methylpyridin-3-amine (15 mg, 0.106 mmol). Isolated compound **54** as an off-white powder (9 mg, 23%): mp: 216–222 °C (dec.); ^{1}H NMR (500 MHz, [D$_6$]DMSO): δ = 10.56 (s, 1H), 9.50 (bs, 1H), 8.44 (d, J = 2.3 Hz, 1H), 8.00 (d, J = 2.3 Hz, 1H), 7.42 (dd, J = 8.4, 2.2 Hz, 1H), 7.34 (d, J = 2.2 Hz, 1H), 7.29 (s, 1H), 7.10 (d, J = 8.5 Hz, 1H), 3.85 (s, 3H), 2.45 ppm (s, 3H); ^{13}C NMR (126 MHz, [D$_6$]DMSO): δ = 171.1, 159.1, 157.8, 152.4, 150.1, 146.9, 144.8, 133.1, 132.2, 127.8, 118.9, 117.9, 112.5, 98.5, 55.7, 20.6 ppm; HRMS (ESI TOF) m/z: $[M+H]^+$ calcd for $C_{17}H_{15}ClN_3O_4$: 360.0746, found: 360.0816.

***N*-(3-Chloro-2-methylphenyl)-5-(4-fluoro-3-hydroxyphenyl)isoxazole-3-carboxamide (60)**: This compound was prepared following the general procedure using 5-(4-fluoro-3-hydroxyphenyl)isoxazole-3-carboxylic acid (29 mg, 0.130 mmol) and 3-chloro-2-methylaniline (18 mg, 0.130 mmol). Isolated compound **60** as an off-white powder (14 mg, 30%): mp: 242–246 °C (dec.); ^{1}H NMR (500 MHz, [D$_6$]DMSO): δ = 10.56 (s, 1H), 10.41 (s, 1H), 7.50 (dd, J = 8.3, 2.2 Hz, 1H), 7.47–7.38 (m, 3H), 7.39–7.31 (m, 2H), 7.28 (t, J = 8.0 Hz, 1H), 2.26 ppm (s, 3H); ^{13}C NMR (126 MHz, [D$_6$]DMSO): δ = 169.9, 158.5 (d, J = 247.1 Hz), 153.5, 151.6, 145.6 (d, J = 12.8 Hz), 136.7, 133.8, 132.1, 127.3, 127.0, 125.9, 123.0 (d, J = 3.4 Hz), 117.8 (d, J = 7.2 Hz), 117.3 (d, J = 19.2 Hz), 114.9 (d, J = 3.6 Hz), 99.9, 15.3 ppm; HRMS (ESI TOF) m/z: $[M+H]^+$ calcd for $C_{17}H_{13}ClFN_2O_3$: 347.0593, found: 347.0597.

***N*-(5-Chloro-2-methylphenyl)-5-(4-fluoro-3-hydroxyphenyl)isoxazole-3-carboxamide (63)**: This compound was prepared following the general procedure (isoxazole amide) **1** using 5-(4-fluoro-3-hydroxyphenyl)isoxazole-3-carboxylic acid (25 mg, 0.112 mmol) and 5-chloro-2-methylaniline (16 mg, 0.112 mmol). Isolated compound **63** as an off-white powder (7 mg, 18%): mp: 214–216 °C (dec.); ^{1}H NMR (500 MHz, [D$_6$]DMSO): δ = 10.36 (s, 1H), 7.51 (dd, J = 7.0, 2.1 Hz, 2H), 7.43 (ddd, J = 8.4, 4.3, 2.2 Hz, 1H), 7.40 (s, 1H), 7.39–7.30 (m, 2H), 7.27 (dd, J = 8.2, 2.3 Hz, 1H), 2.24 ppm (s, 3H); ^{13}C NMR (126 MHz, [D$_6$]DMSO): δ = 169.9, 159.4, 157.3, 152.6 (d, J = 246.5 Hz), 145.8 (d, J = 12.8 Hz), 136.4, 132.3, 131.9, 129.8, 126.1, 125.6, 117.5 (d, J = 7.0 Hz), 117.2 (d, J = 19.3 Hz), 114.9 (d, J = 3.8 Hz), 99.8, 17.2 ppm; HRMS (ESI TOF) m/z: $[M+H]^+$ calcd for $C_{17}H_{13}ClFN_2O_3$: 347.0593, found: 347.0599.

Biology

Reagents. Sucrose, 3-(*N*-morpholino)propanesulfonic acid (MOPS), phosphoric acid, tris(hydroxymethyl)aminomethane (Tris), ethylene glycol tetraacetic acid (EGTA), glutamic acid, malic acid, CsA, phenylarsine oxide (PhAsO), diamide, *N*-ethylmaleimide (NEM), bovine serum albumin (BSA), $CaCl_2$, carbonylcyanide-*p*-trifluoromethoxyphenyl hydrazone (FCCP), verapamil, and dimethyl sulfoxide (DMSO) were from Sigma–Aldrich, CsH was from Enzo Life Sciences, digitonin was from Calbiochem, Rh123 and Calcium Green-5N were from Invitrogen, copper-*o*-phenanthroline ($Cu(OP)_2$) was prepared just before use by mixing $CuSO_4$ with *o*-phenanthroline at a 1:2 molar ratio in double-distilled water. All chemicals were of the highest purity commercially available; 96-well plates were from Sacco S.r.l., Italy.

Animal studies. All procedures were approved by the CEASA of the University of Padova (72/2012 and 39/214 to P.B.) and authorized by the Italian Ministry of Health.

General methodology. Assays on biological samples, including purified mitochondria, cultured cells, and zebrafish were treated with compounds described in this study at a final DMSO concentration of 1%. The compound concentrations stated in biological experiments refer to the "formal" concentration, that is, moles added/volume, making no assumption as to the influence of biological materials on the concentration of added compound.

Isolation of mitochondria. C57BL6/J mouse liver mitochondria were prepared from mice aged between 3 and 6 months by standard differential centrifugation. Mice fed ad libitum were sacrificed by cervical dislocation, their livers were removed and placed in a glass beaker containing ice-cold isolation buffer (IB: 0.25 M sucrose, 10 mM Tris·HCl, 0.1 mM EGTA-Tris, pH 7.4) supplemented with BSA. Livers were then cut into small pieces with scissors, rinsed with ice-cold IB, and passed through a pre-chilled Potter homogenizer with Teflon pestle. The homogenate (~30 mL per liver) was transferred to centrifuge tubes, and unbroken cells and nuclei were removed by centrifugation at 685×*g* for 10 min at 4 °C. The supernatant containing mitochondria and other organelles was transferred to new tubes and centrifuged at 6010×*g* for 10 min at 4 °C. The resulting supernatant was discarded, and mitochondrial pellet was carefully suspended in ice-cold IB buffer and spun at 9390×*g* for 5 min at 4 °C. The pellet was suspended in IB to give a protein concentration of ~60–80 mg mL^{-1} and stored on ice. Experiments were started immediately and completed within 5 h. Protein concentration was determined by the Biuret method.[49]

Cell culture. HeLa cells were grown in Dulbecco's modified Eagle's medium (DMEM) supplemented with 10% fetal bovine serum (Invi-

trogen), 100 U mL^{-1} penicillin and 100 μg mL^{-1} streptomycin (Invitrogen) in a humidified atmosphere of 5% CO_2/95% air at 37 °C.

Assessment of mitochondrial swelling. Changes in mitochondrial volume of isolated mouse liver mitochondria were followed in a 96-well clear assay plate (Falcon 353072) at a final volume of 0.2 mL. First, 0.1 mL of sucrose assay buffer (SAB: 250 mM sucrose, 10 mM MOPS-Tris, 0.01 mM EGTA-Tris, 1.0 mM phosphoric acid-Tris, 10 mM glutamate, and 5 mM malate, pH 7.4) supplemented with twice the Ca^{2+} concentration required to induce mitochondrial swelling (which was determined for each preparation of mitochondria, typically 50 μM) was dispensed to the assay plate. A set of wells also contained 2.0 mM EGTA (to prevent mitochondrial swelling). The test wells contained a range of concentrations of the compounds of interest or 2% DMSO. Experiments were started by the addition of 0.1 mL of mitochondrial suspension (0.5 mg mL^{-1} mitochondria in SAB without respiratory substrates) to the assay plates. Absorbance was read for 30 min at λ 540 nm with a Multi-Skan EX (Thermo Scientific) plate reader.

Assessment of mitochondrial membrane potential. Mitochondrial membrane potential of isolated mouse liver mitochondria was assessed based on accumulation of the cationic fluorescent dye Rh123. First, 0.1 mL of SAB was dispensed to a 96-well black assay plate (Falcon 353376). A set of wells also contained 0.8 μM FCCP (to prevent Rh123 uptake). The test wells contained a range of concentrations of the compounds of interest or 2% DMSO. Then, 0.1 mL of 0.5 mg mL^{-1} mitochondria in SAB devoid of respiratory substrates and supplemented with 0.8 μM Rh123 were added to all wells of the assay plate. Following incubation at room temperature for 5 min, fluorescence intensity (λ_{ex} 485 nm, λ_{em} 538 nm) was read on a Fluoroskan Ascent FL (Thermo Scientific) plate reader.

Assessment of calcium retention capacity. Calcium retention capacity (CRC) of isolated mouse liver mitochondria was assessed as follows: First, 0.1 mL of SAB were dispensed to a 96-well black assay plate (Falcon 353376) in the presence of 2% DMSO (control wells) or varying concentrations of test compounds. Then, 0.1 mL of 0.5 mg mL^{-1} mitochondria in SAB devoid of respiratory substrates but supplemented with 1 μM Calcium Green-5N were added to all wells of the assay plate. A train of 5, 10, or 20 μM Ca^{2+} pulses was added at 1.5, 3, or 4.5 min intervals, respectively, and fluorescence intensity (λ_{ex} 485 nm, λ_{em} 538 nm) was read on Fluoroskan Ascent FL (Thermo Scientific) plate reader.

CRC of HeLa cells. The cells were cultured for 48 h to reach 70–80% confluency, then harvested by trypsinization and washed in KCl buffer (KB: 130 mM KCl, 10 MOPS-Tris, 1 mM phosphoric acid-Tris, 0.1 mM EGTA-Tris, pH 7.4). Cells were then suspended in the above buffer to 8×10^6 cells per mL and treated with 1.56 μM **60** or DMSO on ice for 30 min, followed by excess compound elimination by centrifugation (experiments presented in Figure 4E only; the step was omitted in experiments of Figure 4F). The pellet was resuspended in KB (except that EGTA-Tris was increased to 1.0 mM) to give a concentration of 2×10^7 cells per mL and treated with 0.1 mM digitonin for 10 min on ice to permeabilize the plasma membrane. Following excess digitonin elimination by washing cells twice in KB, the cells were suspended to 8×10^6 cells per mL in KB containing 10 μM EGTA-Tris and supplemented with 1 μM Calcium Green-5N and processed as described for isolated mouse liver mitochondria.

Measurement of respiration. Mitochondrial oxygen consumption was assessed with the Seahorse Extracellular Flux Analyzer XF24 (Seahorse Bioscience, Billerica, MA, USA) essentially as described previously.[50] Briefly, mitochondrial assay solution contained 220 mM mannitol, 70 mM sucrose, 25 mM MOPS-Tris, 10 mM Pi-Tris, 5 mM $MgCl_2$, 1 mM EGTA-Tris, 0.2% fatty-acid-free BSA, 5 mM succinate, and 2 μM rotenone, pH 7.4. Mitochondria (5 μg, suspended in 50 μL mitochondrial assay solution) were added to each well of an XF24 cell culture microplate, centrifuged at 2000×*g* for 20 min at 4 °C, and then supplemented with 450 μL of mitochondrial assay solution containing 4 mM ADP to initiate the experiments. Additions were as indicated in Figure 6A. Cellular oxygen consumption was assessed with the Seahorse Extracellular Flux Analyzer XF24[51] on monolayers of HeLa cells seeded at a density of 3×10^4 per well in 0.2 mL DMEM and cultured for 24 h. Assays were started by replacing the growth medium with 0.5 mL serum and antibiotic-free unbuffered DMEM (pH 7.4) supplemented with the multidrug resistance inhibitor verapamil (20 μM, data not shown) or CsH (2 μg mL^{-1}), and additions were made as indicated in Figure 6C. At the end of the experiment the protein content per well was quantified with a BCA Protein Assay Kit (Thermo Scientific-Pierce).

Cell viability assay. HeLa cells were seeded at a density of 1×10^4 per well in 96-well plates and let to adhere for 6 h before treatment with varying concentrations of **60** or vehicle (1% DMSO) in the presence of the multidrug resistance inhibitor verapamil (20 μM) or CsH (2 μg mL^{-1}). After treatment for 24 h the relative viable cell number was determined with a CellTiter 96 Aqueous One Solution Cell Proliferation Assay Kit (Promega).

Zebrafish and embryo maintenance. Adult zebrafish were maintained in the facility of the University of Padova containing aerated, 28.5 °C-conditioned saline water according to standard protocols. Fish were kept under a 14 h light–10 h dark cycle. For mating, males and females were separated in the late afternoon, and were freed to start courtship the next morning, which ended with egg deposition and fecundation. Eggs were collected, washed with fish water (0.5 mM NaH_2PO_4, 0.5 mM $NaHPO_4$, 0.2 mg L^{-1} methylene blue, 3 mg L^{-1} instant ocean) and embryos were maintained at 28.5 °C. All protocols and manipulations with zebrafish were performed as described.[52]

Morpholino injections. To reproduce the dominant negative UCMD or BM phenotype in zebrafish, we used a previous published exon 9 morpholino,[28] which targets exon 9 of the zebrafish *col6a1* gene. Exon 9, *col6a1*: GAG AGC GGA AGA CGA ACC TTC ATTC (GeneTools, Inc.). A control morpholino, with no sequence homology in zebrafish genome was used. Embryos isolated after paired matings of wild-type zebrafish were injected at 1–2 cell stage using a WPI pneumatic PicoPump PV820 injector. Morpholino was injected at a concentration of 0.1 mM, corresponding to ~4 ng per embryo.

Compound treatment. Morphant embryos were dechorionated at 20 hpf and then treated with 60 at 21 hpf. Untreated morphants and wild-type embryos were used as controls. Compound **60** was used at 5 and 10 μM and dissolved in fish water with 1% DMSO. Vehicle control treatment consisted of fish water with 1% DMSO. Analyses of compound effects on embryos were performed as described at 24 and 48 hpf.

Motor activity. Spontaneous coiling rates were recorded by observing the number of coiling events in 15 s for single embryos at 24 hpf using light microscopy. Touch-evoked escape response was measured at 48 hpf by observing the ability of larvae to escape after touching the body with a little tip. Embryos were subdivided into four groups according to their ability to escape: paralyzed with no ability to move, showing coiling events only, embryos with minor motor impairments, or normal embryos swimming in the fish water; these were assigned a score of 0, 1, 2, or 3, respectively.

Statistical analysis was performed on mean scores at each experimental condition.

Birefringence assay. Muscle birefringence was measured at 48 hpf on tricaine-anesthetized embryos by taking advantage of muscle fiber anisotropy. It was measured using two polarizing filters on a Leica M165FC stereomicroscope. Briefly, anesthetized embryos were placed on a glass slide, and muscle light refraction was analyzed by using two polarizing filters. The first filter produces the polarized light to illuminate the sample, and the second polarizing filter, called the analyzer, calculates the angle of light refracted from muscle fibers. In particular, the top polarizing filter was twisted at a 90° angle until the light refracting through the muscle was visible through a stereomicroscope. Integrated area of birefringence was calculated by using ImageJ software.[48] Birefringence values $\geq 2\times10^6$ (typical of wild-type individuals) were rated as normal, values between 1.9 and 0.6×10^6 were considered as an indication of mild disease, and values $\leq 0.6\times10^6$ were rated as an indication of severe myopathy. Statistical analysis was performed on the mean birefringence values at each experimental condition.

Statistical analysis. Differences between control and compound-treated samples were determined by one-way ANOVA test with Bonferroni correction using GraphPad Prism (version 5.1 for Windows). Data represent the mean of at least five independent experiments ($n=52$ for each condition) $\pm$SEM; $^{**}p<0.01$, $^{***}p<0.001$ for Figure 7A. For Figure 7B, comparison between groups at different conditions was made using χ^2 test and one-way ANOVA with Bonferroni correction; $^{**}p<0.01$, $^{***}p<0.001$. For Figure 7B,C, the total number of embryos used is $n=35$ for each condition; $^{*}p<0.05$, $^{***}p<0.001$, as determined by χ^2 test and one-way ANOVA with Bonferroni correction.

Acknowledgements

The authors gratefully acknowledge funding from the US National Institutes of Health (NIH) and Telethon-Italy. Chemistry efforts at the University of Kansas Specialized Chemistry Center were supported by NIH U54HG005031 awarded to J.A. Support for the University of Kansas NMR instrumentation was provided by NIH Shared Instrumentation Grant number S10RR024664 and National Science Foundation (NSF) Major Research Instrumentation Grant number 0320648. The authors thank Patrick Porubsky (University of Kansas) for compound management. Initial assay validation, high-throughput screening, and hit confirmation efforts at the Conrad Prebys Center for Chemical Genomics were supported by NIH grant U54HG005033 awarded to J.C.R. Funding for the biological assays was provided by NIH R03A033978 awarded to M.F. and P.B., NIH U54HG005031-05S1 awarded to J.A., and by Telethon-Italy GGP14037 to P.B.

Keywords: calcium retention capacity · mitochondria · muscular dystrophy · permeability transition · zebrafish

[1] a) D. Siemen, M. Ziemer, *IUBMB Life* **2013**, *65*, 255 – 262; b) P. Bernardi, A. Rasola, M. Forte, G. Lippe, *Physiol. Rev.* **2015**, *95*, 1111 – 1155.

[2] a) G. Szabadkai, M. R. Duchen, *Physiology* **2008**, *23*, 84 – 94; b) T. E. Gunter, S.-S. Sheu, *Biochim. Biophys. Acta, J. Bioenerg.* **2009**, *1787*, 1291 – 1308.

[3] a) P. Bernardi, A. Krauskopf, E. Basso, V. Petronilli, E. Blachly-Dyson, F. De Lisa, M. Forte, *FEBS J.* **2006**, *273*, 2077 – 2099; b) A. G. Barsukova, D. Bourdette, M. Forte, *Eur. J. Neurosci.* **2011**, *34*, 437 – 447; c) A. Barsukova, A. Komarov, G. Hajnoczky, P. Bernardi, D. Bourdette, M. Forte, *Eur. J. Neurosci.* **2011**, *33*, 831 – 842.

[4] a) P. Bernardi, L. Scorrano, R. Colonna, V. Petronilli, F. Di Lisa, *Eur. J. Biochem.* **1999**, *264*, 687 – 701; b) M. Forte, P. Bernardi, *J. Bioenerg. Biomembr.* **2005**, *37*, 121 – 128.

[5] M. Forte, B. G. Gold, G. Marracci, P. Chaudhary, E. Basso, D. Johnsen, X. Yu, J. Fowlkes, P. Bernardi, D. Bourdette, *Proc. Natl. Acad. Sci. USA* **2007**, *104*, 7558 – 7563.

[6] L. J. Martin, B. Gertz, Y. Pan, A. C. Price, J. D. Molkentin, Q. Chang, *Exp. Neurol.* **2009**, *218*, 333 – 346.

[7] H. Du, L. Guo, F. Fang, D. Chen, A. A. Sosunov, G. M. McKhann, Y. Yan, C. Wang, H. Zhang, J. D. Molkentin, F. J. Gunn-Moore, J. P. Vonsattel, O. Arancio, J. X. Chen, S. D. Yan, *Nat. Med.* **2008**, *14*, 1097 – 1105.

[8] a) D. P. Millay, M. A. Sargent, H. Osinska, C. P. Baines, E. R. Barton, G. Vuagniaux, H. L. Sweeney, J. Robbins, J. D. Molkentin, *Nat. Med.* **2008**, *14*, 442 – 447; b) L. Merlini, A. Angelin, T. Tiepolo, P. Braghetta, P. Sabatelli, A. Zamparelli, A. Ferlini, N. M. Maraldi, P. Bonaldo, P. Bernardi, *Proc. Natl. Acad. Sci. USA* **2008**, *105*, 5225 – 5229.

[9] C. P. Baines, R. A. Kaiser, N. H. Purcell, N. S. Blair, H. Osinska, M. A. Hambleton, E. W. Brunskill, M. R. Sayen, R. A. Gottlieb, G. W. Dorn, J. Robbins, J. D. Molkentin, *Nature* **2005**, *434*, 658 – 662.

[10] A. C. Schinzel, O. Takeuchi, Z. Huang, J. K. Fisher, Z. Zhou, J. Rubens, C. Hetz, N. N. Danial, M. A. Moskowitz, S. J. Korsmeyer, *Proc. Natl. Acad. Sci. USA* **2005**, *102*, 12005 – 12010.

[11] K. Fujimoto, Y. Chen, K. S. Polonsky, G. W. Dorn II, *Proc. Natl. Acad. Sci. USA* **2010**, *107*, 10214 – 10219.

[12] A. Battigelli, J. Russier, E. Venturelli, C. Fabbro, V. Petronilli, P. Bernardi, T. Da Ros, M. Prato, A. Bianco, *Nanoscale* **2013**, *5*, 9110 – 9117.

[13] a) A. W. Leung, P. Varanyuwatana, A. P. Halestrap, *J. Biol. Chem.* **2008**, *283*, 26312 – 26323; b) T. Azarashvili, D. Grachev, O. Krestinina, Y. Evtodienko, I. Yurkov, V. Papadopoulos, G. Reiser, *Cell calcium* **2007**, *42*, 27 – 39.

[14] a) I. Szabó, V. De Pinto, M. Zoratti, *FEBS lett.* **1993**, *330*, 201 – 205; b) I. Szabó, V. De Pinto, M. Zoratti, *FEBS lett.* **1993**, *330*, 206 – 210.

[15] A. P. Halestrap, C. Brennerb, *Curr. Med. Chem.* **2003**, *10*, 1507 – 1525.

[16] a) J. E. Kokoszka, K. G. Waymire, S. E. Levy, J. E. Sligh, J. Cai, D. P. Jones, G. R. MacGregor, D. C. Wallace, *Nature* **2004**, *427*, 461 – 465; b) C. P. Baines, R. A. Kaiser, T. Sheiko, W. J. Craigen, J. D. Molkentin, *Nat. Cell Biol.* **2007**, *9*, 550 – 555.

[17] a) J. Q. Kwong, J. Davis, C. P. Baines, M. A. Sargent, J. Karch, X. Wang, T. Huang, J. D. Molkentin, *Cell Death Differ.* **2014**, *21*, 1209 – 1217; b) M. Gutiérrez-Aguilar, D. L. Douglas, A. K. Gibson, T. L. Domeier, J. D. Molkentin, C. P. Baines, *J. Mol. Cell. Cardiol.* **2014**, *72*, 316 – 325; c) J. Šileikyte, E. Blachly-Dyson, R. Sewell, A. Carpi, R. Menabo, F. Di Lisa, F. Ricchelli, P. Bernardi, M. Forte, *J. Biol. Chem.* **2014**, *289*, 13769 – 13781.

[18] a) V. Giorgio, S. von Stockum, M. Antoniel, A. Fabbro, F. Fogolari, M. Forte, G. D. Glick, V. Petronilli, M. Zoratti, I. Szabo, G. Lippe, P. Bernardi, *Proc. Natl. Acad. Sci. USA* **2013**, *110*, 5887 – 5892; b) M. Carraro, V. Giorgio, J. Sileikyte, G. Sartori, M. Forte, G. Lippe, M. Zoratti, I. Szabo, P. Bernardi, *J. Biol. Chem.* **2014**, *289*, 15980 – 15985.

[19] P. Bernardi, *Front. Physiol.* **2013**, *4*, 95.

[20] For a detailed discussion on prior art, see reference [29].

[21] E. Basso, L. Fante, J. Fowlkes, V. Petronilli, M. Forte, P. Bernardi, *J. Biol. Chem.* **2005**, *280*, 18558 – 18561.

[22] P. Wang, J. Heitman, *Genome Biol.* **2005**, *6*, 226.

[23] J. Liu, J. D. Farmer, Jr., W. S. Lane, J. Friedman, I. Weissman, S. L. Schreiber, *Cell* **1991**, *66*, 807 – 815.

[24] P. C. Waldmeier, J. J. Feldtrauer, T. Qian, J. J. Lemasters, *Mol. Pharmacol.* **2002**, *62*, 22 – 29.

[25] a) E. P. Taddeo, R. C. Laker, D. S. Breen, Y. N. Akhtar, B. M. Kenwood, J. A. Liao, M. Zhang, D. J. Fazakerley, J. L. Tomsig, T. E. Harris, S. R. Keller, J. D. Chow, K. R. Lynch, M. Chokki, J. D. Molkentin, N. Turner, D. E. James, Z. Yan, K. L. Hoehn, *Mol. Metab.* **2014**, *3*, 124 – 134; b) T. Tiepolo, A. Angelin, E. Palma, P. Sabatelli, L. Merlini, L. Nicolosi, F. Finetti, P. Braghetta, G. Vuagniaux, J. M. Dumont, C. T. Baldari, P. Bonaldo, P. Bernardi, *Br. J. Pharmacol.* **2009**, *157*, 1045 – 1052.

[26] a) A. H. Schinkel, E. Wagenaar, L. van Deemter, C. A. Mol, P. Borst, *J. Clin. Invest.* **1995**, *96*, 1698 – 1705; b) S. Murasawa, K. Iuchi, S. Sato, T. Noguchi-Yachide, M. Sodeoka, T. Yokomatsu, K. Dodo, Y. Hashimoto, H. Aoyama, *Bioorg. Med. Chem.* **2012**, *20*, 6384 – 6393; c) B. Yun, H. Lee, M.

Ghosh, B. F. Cravatt, K. L. Hsu, J. V. Bonventre, H. Ewing, M. H. Gelb, C. C. Leslie, *J. Biol. Chem.* **2014**, *289*, 1491 – 1504.

[27] D. Fancelli, A. Abate, R. Amici, P. Bernardi, M. Ballarini, A. Cappa, G. Carenzi, A. Colombo, C. Contursi, F. Di Lisa, G. Dondio, S. Gagliardi, E. Milanesi, S. Minucci, G. Pain, P. G. Pelicci, A. Saccani, M. Storto, F. Thaler, M. Varasi, M. Villa, S. Plyte, *J. Med. Chem.* **2014**, *57*, 5333 – 5347.

[28] a) W. R. Telfer, A. S. Busta, C. G. Bonnemann, E. L. Feldman, J. J. Dowling, *Hum. Mol. Genet.* **2010**, *19*, 2433 – 2444; b) A. Zulian, E. Rizzo, M. Schiavone, E. Palma, F. Tagliavini, B. Blaauw, L. Merlini, N. M. Maraldi, P. Sabatelli, P. Braghetta, P. Bonaldo, F. Argenton, P. Bernardi, *Hum. Mol. Genet.* **2014**, *23*, 5353 – 5363.

[29] "Small Molecules Targeting the Mitochondrial Permeability Transition", J. Sileikyte, S. Roy, P. Porubsky, B. Neuenswander, J. Wang, M. Hedrick, A. B. Pinkerton, S. Salaniwal, P. Kung, A. Mangravita-Novo, L. H. Smith, D. N. Bourdette, M. R. Jackson, J. Aubé, T. D. Chung, F. J. Schoenen, M. F. Forte, P. Bernardi in: *NIH Molecular Libraries. Probe Reports from the Molecular Libraries Program* [http://www.ncbi.nlm.nih.gov/books/NBK47352/: April 15, 2014 (updated January 16, 2015)], Bethesda (MD), National Center for Biotechnology Information (USA), 2010.

[30] a) J. B. Baell, *Future Med. Chem.* **2010**, *2*, 1529 – 1546; b) J. B. Baell, G. A. Holloway, *J. Med. Chem.* **2010**, *53*, 2719 – 2740.

[31] K. A. Kumar, P. Jayaroopa, *Int. J. Pharm. Chem. Biol. Sci.* **2013**, *3*, 294 – 304.

[32] H. K. Jung, M. R. Doddareddy, J. H. Cha, H. Rhim, Y. S. Cho, H. Y. Koh, B. Y. Jung, A. N. Pae, *Bioorg. Med. Chem.* **2004**, *12*, 3965 – 3970.

[33] S. R. Bertenshaw, J. S. Carter, P. W. Collins, S. H. Docter, M. J. Granets, I. K. Khanna, J. W. Malecha, J. M. Miyashiro, T. D. Penning, K. L. Rogers, D. J. Rogier, Jr., J. J. Talley, S. S. Yu (G.D. Searle & Co.), Pat. No. EP 0924201 B1, **1999**.

[34] A. Bischoff, K. Sundaresan, R. P. Bala Koteswara, B. Ainan, H. Ayyamperumal, R. Grish A., S. Tatiparthy, G. Prabhu, H. Subramanya (Forest Laboratories Holdings Ltd.), Int. PCT Pub. No. WO 2009117676 A3, **2010**.

[35] A. L. Hopkins, G. M. Keseru, P. D. Leeson, D. C. Rees, C. H. Reynolds, *Nat. Rev. Drug Discovery* **2014**, *13*, 105 – 121.

[36] Full panel inhibition data for compound **60** are provided in the Supporting Information.

[37] a) L. Azzolin, S. von Stockum, E. Basso, V. Petronilli, M. A. Forte, P. Bernardi, *FEBS lett.* **2010**, *584*, 2504 – 2509; b) S. von Stockum, V. Giorgio, E. Trevisan, G. Lippe, G. D. Glick, M. A. Forte, C. Da-Re, V. Checchetto, G. Mazzotta, R. Costa, I. Szabo, P. Bernardi, *J. Biol. Chem.* **2015**, *290*, 4537 – 4544; c) F. Ricchelli, F. Dabbeni-Sala, V. Petronilli, P. Bernardi, B. Hopkins, S. Bova, *Biochim. Biophys. Acta Bioenerg.* **2005**, *1708*, 178 – 186.

[38] V. Petronilli, P. Costantini, L. Scorrano, R. Colonna, S. Passamonti, P. Bernardi, *J. Biol. Chem.* **1994**, *269*, 16638 – 16642.

[39] a) P. Costantini, R. Colonna, P. Bernardi, *Biochim. Biophys. Acta Bioenerg.* **1998**, *1365*, 385 – 392; b) J. Sileikyte, V. Petronilli, A. Zulian, F. Dabbeni-Sala, G. Tognon, P. Nikolov, P. Bernardi, F. Ricchelli, *J. Biol. Chem.* **2011**, *286*, 1046 – 1053.

[40] a) J. M. Ford, W. N. Hait, *Pharmacol. Rev.* **1990**, *42*, 155 – 199; b) P. Bernardi, *Ital. J. Neurol. Sci.* **1999**, *20*, 395 – 400.

[41] a) T. Tsuruo, H. Iida, S. Tsukagoshi, Y. Sakurai, *Cancer Res.* **1981**, *41*, 1967 – 1972; b) I. Bosch, J. Croop, *Biochim. Biophys. Acta Rev. Cancer* **1996**, *1288*, F37 – F54.

[42] a) G. Pepe, E. Bertini, P. Bonaldo, K. Bushby, B. Giusti, M. de Visser, P. Guicheney, G. Lattanzi, L. Merlini, F. Muntoni, I. Nishino, I. Nonaka, R. B. Yaou, P. Sabatelli, C. Sewry, H. Topaloglu, A. van der Kooi, *Neuromuscular Disord.* **2002**, *12*, 984 – 993; b) A. K. Lampe, K. M. D. Bushby, *J. Med. Genet.* **2005**, *42*, 673 – 685.

[43] a) N. M. Maraldi, P. Sabatelli, M. Columbaro, A. Zamparelli, F. A. Manzoli, P. Bernardi, P. Bonaldo, L. Merlini, *Adv. Enzyme Regul.* **2009**, *49*, 197 – 211; b) W. A. Irwin, N. Bergamin, P. Sabatelli, C. Reggiani, A. Megighian, L. Merlini, P. Braghetta, M. Columbaro, D. Volpin, G. M. Bressan, P. Bernardi, P. Bonaldo, *Nat. Genet.* **2003**, *35*, 367 – 371.

[44] A. Angelin, T. Tiepolo, P. Sabatelli, P. Grumati, N. Bergamin, C. Golfieri, E. Mattioli, F. Gualandi, A. Ferlini, L. Merlini, N. M. Maraldi, P. Bonaldo, P. Bernardi, *Proc. Natl. Acad. Sci. USA* **2007**, *104*, 991 – 996.

[45] a) A. Zulian, F. Tagliavini, E. Rizzo, C. Pellegrini, F. Sardone, N. Zini, N. M. Maraldi, S. Santi, C. Faldini, L. Merlini, V. Petronilli, P. Bernardi, P. Sabatelli, *Front. Aging Neurosci.* **2014**, *6*, 324; b) L. Merlini, P. Sabatelli, A. Armaroli, S. Gnudi, A. Angelin, P. Grumati, M. E. Michelini, A. Franchella, F. Gualandi, E. Bertini, N. M. Maraldi, A. Ferlini, P. Bonaldo, P. Bernardi, *Oxid. Med. Cell. Longevity* **2011**, *2011*, 139194.

[46] E. Palma, T. Tiepolo, A. Angelin, P. Sabatelli, N. M. Maraldi, E. Basso, M. A. Forte, P. Bernardi, P. Bonaldo, *Hum. Mol. Genet.* **2009**, *18*, 2024 – 2031.

[47] a) L. Lucarini, B. Giusti, R.-Z. Zhang, T.-C. Pan, C. Jimenez-Mallebrera, E. Mercuri, F. Muntoni, G. Pepe, M.-L. Chu, *Hum. Genet.* **2005**, *117*, 460 – 466; b) A. K. Lampe, Y. Zou, D. Sudano, K. K. O'Brien, D. Hicks, S. H. Laval, R. Charlton, C. Jimenez-Mallebrera, R. Z. Zhang, R. S. Finkel, G. Tennekoon, G. Schreiber, M. S. van der Knaap, H. Marks, V. Straub, K. M. Flanigan, M. L. Chu, F. Muntoni, K. M. D. Bushby, C. G. Bönnemann, *Hum. Mutat.* **2008**, *29*, 809 – 822.

[48] J. Berger, T. Sztal, P. D. Currie, *Biochem. Biophys. Res. Commun.* **2012**, *423*, 785 – 788.

[49] A. G. Gornall, C. J. Bardawill, M. M. David, *J. Biol. Chem.* **1949**, *177*, 751 – 766.

[50] G. W. Rogers, M. D. Brand, S. Petrosyan, D. Ashok, A. A. Elorza, D. A. Ferrick, A. N. Murphy, *PloS one* **2011**, *6*, e21746.

[51] M. Wu, A. Neilson, A. L. Swift, R. Moran, J. Tamagnine, D. Parslow, S. Armistead, K. Lemire, J. Orrell, J. Teich, S. Chomicz, D. A. Ferrick, *Am. J. Physiol.* **2006**, *292*, C125 – C136.

[52] C. B. Kimmel, W. W. Ballard, S. R. Kimmel, B. Ullmann, T. F. Schilling, *Dev. Dyn.* **1995**, *203*, 253 – 310.

Received: June 30, 2015
Published online on August 18, 2015